

Comparison of TOA and BOA LW radiation fluxes inferred from ground-based sensors, A-Train satellite observations and ERA reanalyses at the High Arctic Station Eureka over the 2002 to 2020 period

Yann Blanchard¹, Jacques Pelon², Christopher J Cox³, Julien Delanoë⁴, Edwin W Eloranta⁵, and Taniel Uttal⁶

¹ESCER Centre

²LATMOS/IPSL

³CIRES/NOAA-ESRL

⁴Laboratoire ATmosphère, Milieux, et Observations Spatiales (LATMOS), IPSL/UVSQ/CNRS

⁵University of Wisconsin

⁶NOAA ETL

November 22, 2022

Abstract

This paper focuses on the accuracy of longwave radiation flux retrievals at the top and bottom of the atmosphere at Eureka station, Canada, in the high Arctic. We report comparisons between seven products derived from (1) calculations based on a combination of ground-based and space-based lidar and radar observations, (2) standard radiometric observations from the CERES satellite, (3) direct observations at the surface from a broadband radiation station and (4) the ERA-Interim and ERA5 reanalyses. Statistical, independent analyses are first performed to look at recurring bias and trends in fluxes at Top and Bottom of the Atmosphere. The analysis is further refined comparing fluxes derived from coincident observations decomposed by scene types. Results show that radiative transfer calculations using ground-based lidar-radar profiles derived at Eureka agree well with TOA LW fluxes observed by CERES and with BOA LW fluxes reference. CloudSat-CALIPSO also show good agreement with calculations from ground-based sensor observations, with a relatively small bias. This bias is shown to be largely due to low and thick cloud occurrences that the satellites are insensitive to owing to attenuation from clouds above and surface clutter. These conditions of opaque low clouds, cause an even more pronounced bias for CERES BOA flux calculation in winter, due to the deficit of low clouds identified by MODIS. ERA-I and ERA5 fluxes behave differently, the large positive bias observed with ERA-I is much reduced in ERA5. ERA5 is closer to reference observations due to a better behaviour of low and mid-level clouds.

1 **Comparison of TOA and BOA LW radiation fluxes inferred from ground-based**
2 **sensors, A-Train satellite observations and ERA reanalyses at the High Arctic Station**
3 **Eureka over the 2002 to 2020 period**
4

5 **Yann Blanchard¹, Jacques Pelon², Christopher J. Cox^{3,4}, Julien Delanoë², Edwin W.**
6 **Eloranta⁵ and Taniel Uttal⁴**

7 ¹Centre pour l'Étude et la Simulation du Climat à l'Échelle Régionale (ESCER), Université du
8 Québec à Montréal, Montréal, Québec, Canada.

9 ²Laboratoire Atmosphères, Milieux, Observations Spatiales, SU-UVSQ-CNRS, Paris, France.

10 ³Cooperative Institute for Research in Environmental Sciences (CIRES), University of Colorado,
11 National Oceanic and Atmospheric Administration (NOAA), Boulder, Colorado, USA.

12 ⁴Physical Sciences Division, NOAA, Boulder, Colorado, USA.

13 ⁵Space Science and Engineering Center, University of Wisconsin–Madison, Madison,
14 Wisconsin, USA.

15
16 Corresponding author: Yann Blanchard (yann.blanchard@usherbrooke.ca)

17
18
19 **Key Points:**

- 20 • Top-Of-Atmosphere flux observations, model calculations and reanalyses agree within
21 the measurement uncertainty at a High Arctic Station
- 22 • Large Bottom-Of-Atmosphere biases are observed among datasets and are mainly due to
23 incorrect vertical representation of low opaque clouds
- 24 • Ground-based active sensors are essential to complement space-based cloud observations
25 in order to better understand Arctic climate change
26

27 **Abstract**

28 This paper focuses on the accuracy of longwave radiation flux retrievals at the top and
29 bottom of the atmosphere at Eureka station, Canada, in the high Arctic. We report comparisons
30 between seven products derived from (1) calculations based on a combination of ground-based
31 and space-based lidar and radar observations, (2) standard radiometric observations from the
32 CERES satellite, (3) direct observations at the surface from a broadband radiation station and (4)
33 the ERA-Interim and ERA5 reanalyses. Statistical, independent analyses are first performed to
34 look at recurring bias and trends in fluxes at Top and Bottom of the Atmosphere. The analysis is
35 further refined comparing fluxes derived from coincident observations decomposed by scene
36 types. Results show that radiative transfer calculations using ground-based lidar-radar profiles
37 derived at Eureka agree well with TOA LW fluxes observed by CERES and with BOA LW
38 fluxes reference. CloudSat-CALIPSO also show good agreement with calculations from ground-
39 based sensor observations, with a relatively small bias. This bias is shown to be largely due to
40 low and thick cloud occurrences that the satellites are insensitive to owing to attenuation from
41 clouds above and surface clutter. These conditions of opaque low clouds, cause an even more
42 pronounced bias for CERES BOA flux calculation in winter, due to the deficit of low clouds
43 identified by MODIS. ERA-I and ERA5 fluxes behave differently, the large positive bias
44 observed with ERA-I is much reduced in ERA5. ERA5 is closer to reference observations due to
45 a better behaviour of low and mid-level clouds.

47 **Plain Language Summary**

48 Satellite and reanalysis datasets are widely used for climate and process studies in the
49 Arctic in order to complement sparse ground-based measurements. This study compares ground-
50 based observations of Arctic clouds and longwave fluxes at a Canadian High Arctic station with
51 satellite and reanalysis products. Both statistical and coincident analyses show a good top of the
52 atmosphere agreement, but reveal biases in surface fluxes that are due to the underestimation of
53 the occurrence of low and thick clouds, frequent in the Arctic. The results allow for an evaluation
54 of flux product uncertainties and for an assessments of their limitations. The outcomes of this
55 study can be applied over the entire Arctic region and can inform the instrumentation choices at
56 various polar ground-based sites.

57 **1 Introduction**

58 Interest in the Arctic climate has increased as the effects of global warming have begun
59 to manifest in the region over the several decades (IPCC, 2013). These manifestations include
60 increases in surface temperature that are larger than those observed at lower latitudes (McBean,
61 2005; Comiso et Hall, 2014); significant decreases in sea-ice extent and thickness (Palm et al.,
62 2010, Serreze and Barry, 2011; Lang et al., 2017); and changes in Arctic cloud cycle and
63 interactions (Sedlar et al., 2011; Liu et al., 2012; Abe et al., 2016). Large scale meteorological
64 dynamical forcings on a more fragile sea-ice interface impact surface energy budgets and modify
65 ice properties. Transport of aerosols (Rahn, 1981, Ancellet et al., 2014, Igel et al., 2017) and
66 larger water vapor intrusions from lower latitudes (Doyle et al., 2011, Boisvert et al., 2015; Liu
67 et al., 2018) can affect cloud cycle and precipitation, as well as cloud radiative effects (Cox et al.,
68 2015). Cloud radiation, especially from low-level clouds is a key component of the energy
69 budget at the surface (Serreze and Barry, 2014; Sedlar et al., 2011; Sedlar et al, 2012; Shupe et
70 al., 2013, English et al., 2015), and such clouds are directly impacted by the aforementioned

71 atmospheric variability. A better understanding of feedbacks controlling Arctic change and the
72 need for improved models (English et al., 2015, Kay et al., 2016, Li and Xu, 2020) emphasize
73 the need to better constrain models with observations. To achieve this, particular attention must
74 be given to the autumn-winter-spring period, during which transport of warmer and moister air
75 masses from mid-latitudes may enhance sea-ice decline (Graham et al., 2017), including through
76 modulation of longwave and shortwave cloud effects (Cox et al. 2016).

77
78 There are only a small number of surface land stations in the pan-Arctic region dedicated
79 to atmospheric research (Uttal et al., 2016), and only a subset of these regularly make
80 measurements using active instrumentation such as radar and lidar, which are necessary to
81 retrieve cloud properties with vertical resolution. These retrieved profiles are valuable for
82 understanding the vertical distribution and properties of cloud layers necessary to accurately
83 model radiative transfer through the atmosphere (Shupe et al., 2013; Shupe et al., 2015a; Shupe
84 et al., 2015b). The stations are located over land and many are coastal. Thus, data may be subject
85 to spatial heterogeneity characteristic of such environments (e.g., orographic effects, specific
86 atmospheric or ocean circulation flows, variable surface reflectivity) and so may not be
87 representative at the regional scale (Eastman and Warren 2010, Shupe et al. 2011a). New stations
88 (drifting buoys) are being implemented over the Arctic ocean (Provost et al., 2015; Mariage et
89 al., 2017), that should bring new information on aerosol and cloud profiles as well as the Surface
90 Radiation Budget (SRB), together providing a regional support to characterize SRB in
91 combination with space observations. However, observations from Clouds and the Earth's
92 Radiant Energy System–Energy Balanced and Filled (CERES-EBAF) (Loeb et al., 2009) have
93 long been the only available radiative flux information over the Arctic Ocean. The advent of
94 polar-orbiting satellite active sensors, with the success of CALIPSO/CloudSat missions
95 (Stephens et al., 2018), allows for a more precise estimation of the regional Arctic cloud cover,
96 quantification of cloud type vertical distribution, and inference of radiative fluxes at the regional
97 scale (Kay and L'Ecuyer, 2013; Kay et al., 2016). The upcoming EarthCARE mission is
98 designed to pursue and reinforce this progress through a continued instrumental synergy
99 (Illingworth et al., 2015). However, while satellites provide the spatial coverage lacking from the
100 surface stations, they do not directly observe the surface radiation budget and so must be
101 validated.

102
103 Extensive characterization of Arctic SRB therefore necessitates a combination of the
104 ground-based and satellite retrievals and a more accurate evaluation of all biases through
105 comprehensive intercomparisons between observations. Previous work emphasized that the use
106 of passive instruments (e.g. MODIS) alone is insufficient because of underestimation of cloud
107 fraction in winter and autumn (Liu, 2010, Blanchard et al., 2014, hereinafter B14). As cloud
108 products from satellite are commonly used to contribute to atmospheric reanalysis and to
109 compute cloud radiative forcing, errors in cloud detection or biases in cloud products, as shown
110 in Liu and Key (2016), may lead to errors in flux calculations. Consequently, B14 concluded that
111 spaceborne lidar–radar synergy is essential for a complete representation of the cloud vertical
112 profile, but that both surface and space observations are needed to reduce biases in all
113 observations. Near-surface clouds are frequent in central Arctic (Uttal et al., 2002; Mariage et al,
114 2017). Below about 1 km in altitude, space-based radar observations are inhibited by ground
115 clutter (Palermé et al., 2019). Conversely, lidar sensitivity may be limited below clouds by
116 attenuation, enhanced in presence of supercooled layers at cloud top. B14 found that the

117 characterization of low clouds as well as boundary layer events (composed of aerosols and/or
118 precipitating ice crystals) are two of the principal challenges for spaceborne observations and the
119 determination of radiation fluxes at the surface.

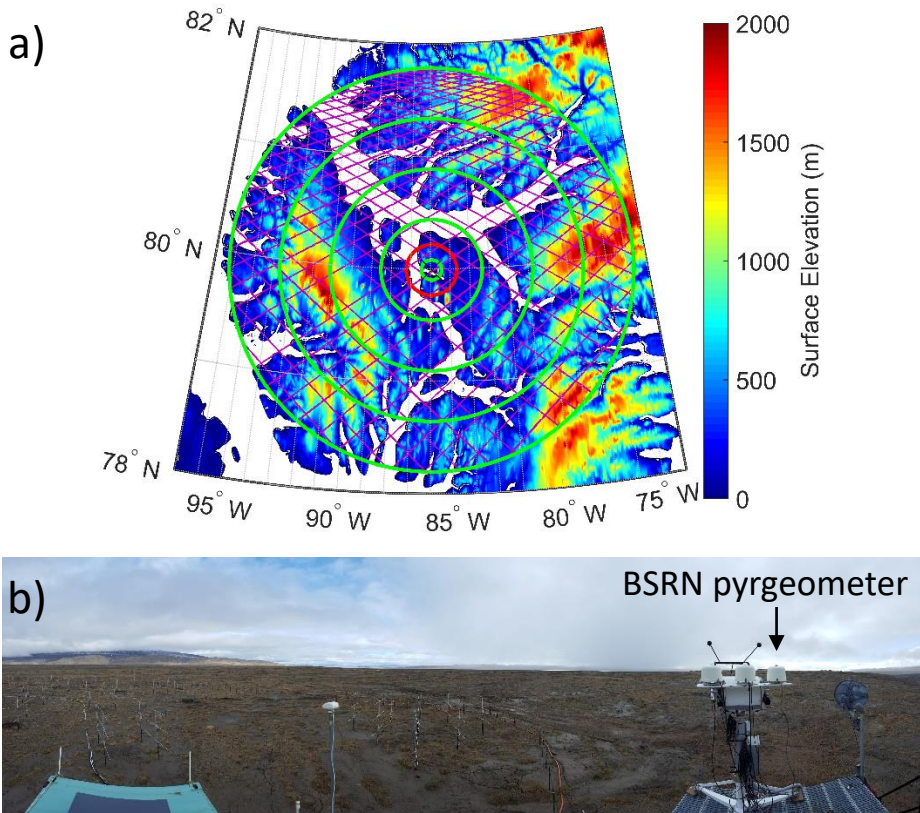
120
121 Longwave (LW) radiation is an important component of the energy budget in the Arctic
122 and is indeed the only radiative flux during polar night. LW is additionally particularly sensitive
123 to the profile of atmospheric and cloud properties and therefore products such as CERES-EBAF
124 are very sensitive to errors in the profiles from which the calculations of the fluxes are made. In
125 this paper, we focus on the retrieval of LW radiation fluxes both at the top of atmosphere (TOA)
126 and at the bottom of atmosphere (BOA), as observed from the ground and from space and
127 simulated from radiative transfer models over Eureka, Nunavut, Canada (80 °N, 86 °W). Eureka
128 is a high-Arctic surface observatory with 5 years of overlapping measurements from the
129 necessary instrumentation and is representative of a particularly dry region of the Arctic (Cox et
130 al. 2012) where clouds are distributed over a wider range of heights than other locations (Shupe
131 et al. 2011a). The instrumentation and the time series of records at Eureka site has allowed a
132 significant number of studies related to climate (Lesins et al., 2010; Cox et al., 2012),
133 comparisons of cloud cover (de Boer, 2009; Shupe, 2011a, 2011b, B14) and downwelling fluxes
134 (Cox et al., 2012). According to this latter study, the yearly average downwelling LW cloud
135 radiative effect (difference of cloudy and clear air downwelling fluxes) at the bottom of the
136 atmosphere (BOA) at Eureka is about 27 W/m². The aim of this work is to analyze radiative flux
137 comparisons following an approach similar to the one developed in B14. Namely, we perform
138 two main analyses on a statistical basis using independent and coincident observations involving
139 vertical profiles and cloud retrievals from a synergistic use of lidar and radar data. We interpret
140 results generally to draw conclusions applicable to the performance of the products under
141 particular atmospheric regimes.

142
143 We first present upwelling and downwelling LW fluxes derived from satellite and surface
144 observations, including calculations using cloud profile measurements at Eureka. All
145 observations are compared to the ERA-Interim and ERA5 reanalyses of the European Center for
146 Medium Weather Forecast (ECMWF). Comparisons of seasonal variations of fluxes from
147 statistical analyses and cloud vertical distribution based on independent datasets are detailed in
148 section 3. On the basis of the coincident data, comparison of flux distributions and their
149 differences are then discussed in section 4. Finally, we discuss the results of the comparisons and
150 identify biases and limitations.

151 **2 Description of observation site and datasets**

152 The focus surface observation site are the Zero Altitude PEARL Auxiliary Laboratory
153 (OPAL) and the Surface and Atmospheric Flux, Irradiance and Radiation Extension (SAFIRE),
154 both part of the Polar Environment Atmospheric Research Laboratory (PEARL; Fogal et al.,
155 2013) in Eureka, Nunavut, Canada, which is one of the high-latitude stations of the Network for
156 the Detection of Atmospheric Composition Change (NDACC, http://www.ndsc.ncep.noaa.gov/sites/stat_reps/eureka/). It is also part of the IASOA network
157 (Uttal et al. 2016), and, located at SAFIRE, a World Radiation Monitoring Center Baseline
158 Surface Radiation Network (WCRP-BSRN, <http://bsrn.awi.de/>) station during the study period,
159 2007 and 2011 (Dreimel et al. 2018). Ground-truthing of satellite studies is one of the principle
160 objectives of BSRN. Note that while the radiosonde launch facility, as well as the lidar and radar
161

162 instruments are located close to sea level at OPAL, SAFIRE is located approximately 5 km
 163 northeast at 85 m (asl). Eureka is situated in the northernmost part of the Canadian Arctic
 164 Archipelago, a region having complex topography and variable surface type. However, despite
 165 this heterogeneity, the station offers a critical mass of observations and because of its latitude
 166 also a high frequency of satellite overpasses, enabling a larger number of coincident samples to
 167 be analyzed (B14). Figure 1 shows a map of Ellesmere and Axel Heiberg islands with the
 168 location of the Eureka station marked on the western coast of Ellesmere as well as a photograph
 169 of the BSRN station highlighting flat, open area chosen for siting SAFIRE.
 170



171
 172 **Figure 1.** (a) A-Train tracks (in magenta) close to the Eureka station (black cross) during
 173 January 2007 superposed over the digital elevation model Global 30 arc s elevation dataset
 174 (GTOPO30) used for CALIPSO data analysis. The green concentric circles (radius of 10, 25, 50,
 175 100, 150 and 200 km) denote the area of this study. The 25 (red) circle delimits domains where
 176 surface orography and heterogeneity are minimized. (b) Panoramic view of the Eureka radiation
 177 site (SAFIRE) where the pyrgeometer is located.

178
 179 Kovacs and McCormick (2005) suggest that for cloud-comparison purposes a length
 180 scale of a few tens of kilometers and a time scale of a few minutes is sufficient for identifying
 181 coincident observations. Based on this recommendation, we will define 25 km from Eureka as
 182 the maximum distance for the current study, which is also similar to the grid size of ERA-I,
 183 ERA5 and CERES. The region where spaceborne observations are analyzed is also shown in
 184 Figure 1.

185

186 CERES and MODIS have collected measurements since 1999 and 2002 onboard TERRA
 187 and AQUA, respectively. CloudSat and CALIPSO (hereafter referred to as C-C) were launched
 188 in 2006 and are part of the constellation of satellites formed with AQUA (A-Train). CloudSat has
 189 made measurements only during daytime since 2011 due to a battery anomaly and the production
 190 of CloudSat 2B-FLXHR-LIDAR products (hereafter C-C-FLX) was discontinued at that time.
 191 Two releases of this product (R04 and R05) are however available from 2006 and almost over
 192 the same period. Although considering the whole period from 2002 to 2020 for the overall
 193 statistical analysis, the period of detailed analysis on coincident observations is limited to the
 194 overlap period spanning from June 2006 to May 2010, due to the availability of radiation
 195 products.

196
 197 Table 1 summarizes the main characteristics of the datasets and methods used in this
 198 study.

199
 200 **Table 1.** Satellite, ground-based and reanalysis data sets and methods used in this study

Name	CERES	C-C-FLX	ERA-I / ERA5	EUR-LR	BSRN
Long name	CERES_SSF_Aqua-XTRK_Edition4A	CloudSat 2B-FLXHR-LIDAR	ECMWF ERA-Interim / ERA5	EUREKA-LIDAR-RADAR	Baseline Surface Radiation Network
Version	Edition 4A	Release 04 and 05			
Temporal resolution	2 – 4 s	0.16 s	3h	3 min	1 min
Vertical resolution	N/A	240 m	137 levels	30 m	N/A
Footprint	20 km x 20 km	1.4 km x 1.7 km	0.125°x 0.125°	N/A	N/A
Cloud properties	MODIS Collection 5 cloud products	CloudSat and CALIPSO	Reanalysis	From radar-lidar synergy	N/A
TOA fluxes	Observed	BugsRad RTM	Reanalysis	Streamer RTM	
BOA fluxes	Longwave Model B	BugsRad RTM	Reanalysis	Streamer RTM	Observed
References	Wielicki et al., 1996 Loeb et al., 2018	Henderson et al., 2013	Dee et al., 2011 Hersbach and Dee, 2016	Donovan and van Lammeren (2001); Shupe (2007)	McArthur, 2005; Driemel et al., 2018

201

202 2.1 Fluxes from ground-based observations

203 Profiles of cloud properties are regularly measured above Eureka from combined radar
 204 and lidar measurements (B14). Here, we use these data as reference for heights of cloud layers
 205 over the site. TOA and BOA fluxes based on the lidar and radar measurements at Eureka
 206 (hereafter “EUR-L-R”) were calculated using the Streamer radiative transfer code (Key and
 207 Schweiger, 1988). The input parameters include atmospheric profiles (interpolated from twice
 208 daily radiosonde measurements), aerosol optical depth from the Eureka sunphotometer (part of
 209 AERONET, <https://aeronet.gsfc.nasa.gov/>), and cloud layer information (type of layer, altitude,

210 layer optical depth, and mean effective radius) from ground-based lidar and radar (as detailed in
211 Blanchard et al., 2017). Cloud type was derived from a multisensor classifier (Shupe, 2007) and
212 particle sizes were retrieved from the ratio of radar and lidar backscatter cross-section (Eloranta
213 et al., 2007) using default processing on the web site <http://hsrl.ssec.wisc.edu>. The purpose of
214 this product is to be a comparable analog to the CloudSat and CALIPSO products, but from the
215 perspective of the surface.

216

217 The LW flux data from the BSRN station are 1-minute averages based on 1 Hz samples
218 collected by a shaded Eppley pyrgeometer mounted on a sun tracker (Driemel et al., 2018).
219 Grachev et al. (2018) reported on the intercomparability of the BSRN LW for an overlap period
220 with another radiometer approximate 700 m east of the BSRN station at Eureka and found a
221 negligible bias ($\sim 1 \text{ W/m}^2$) and with a standard deviation of 10.5 W/m^2 in the differences of
222 hourly means.

223

224 The BSRN pyrgeometer was maintained approximately at daily intervals. In cold
225 climates this maintenance includes manual removal of ice from the sensor windows, which
226 commonly occurs. The pyrgeometer was ventilated, which helps maintain temperature stability
227 and mitigate the formation of ice. Unfortunately, despite these procedures, icing of the window
228 frequently occurred on the pyrgeometer throughout the study period. Because the specific post-
229 processing procedures used on the data archived at BSRN are undocumented, we began with the
230 raw data set and conducted our own quality control, including implementing the procedures
231 recommended by Long and Shi (2008) as well as visual screening for signs of icing. The signal
232 from the iced window is similar to the signal from clouds, making it difficult to identify. For an
233 upward-facing LW measurement, the bias caused by the ice is generally positive, and is large
234 when the sky is clear and small when the sky is cloudy. Manual removal of ice by the technicians
235 causes a change in the signal that is very fast compared to natural variability and this non-
236 physical signal is easily identifiable, as is the decrease in radiance following the growth curve of
237 the developing ice that precedes the cleaning backward in time. By identifying and removing
238 these features, the visual screening likely removed most of the ice that occurred when the sky
239 was radiatively clear and the bias was large, but the subsequent absence of the radiatively clear
240 time periods in the record produces a climatological bias in the monthly means. Monthly means
241 are only used in this study for qualitative purposes so it was more important to have a
242 representative estimate than a direct measurement for these periods. We therefore filled the gaps
243 from the data removed because of icing with a calculation of the clear-sky downwelling LW
244 following Long and Turner (2008), which is based on Brutsaert's equation and requires only the
245 radiometric measurements and collocated meteorology. Time periods that use these estimates are
246 not incorporated into the validation analysis of this study. The subset of observations coincident
247 with the satellite overpasses that are used for comparison received further scrutiny individually,
248 including analysis of logbook records, radar and lidar data, meteorology and the other
249 radiometric data in order to identify and remove additional suspect data that remained. This
250 procedure had the added benefit of being well-suited to identify times where comparisons were
251 likely to be influenced by cloud cover that was within the $\sim 160^\circ$ effective FOV of the
252 pyrgeometer at times when the skies directly over Eureka were clear. Appendix A presents
253 results from this data screening.

254

255 2.2 Fluxes from satellite

256 Radiation measurements from the CERES instrument on AQUA and TERRA provide a
257 direct observation of the upwelling TOA radiances (Wielicki et al., 1996), that are converted into
258 fluxes using angular distribution models that provide a stable time series (Loeb et al., 2012).
259 Specific comparisons of the Clouds and the Earth’s Radiant Energy System–Energy Balanced
260 and Filled (CERES-EBAF) TOA fluxes (Loeb et al., 2009) have been performed at high latitudes
261 over the Arctic (Kay et al., 2013, Huang et al., 2017b). CERES provides access to a long and
262 homogeneous radiation database, and has been used in numerous analyses. Based on these
263 considerations, the AQUA CERES-SSF TOA fluxes (V4.0) were taken as a reference for
264 comparisons in the present study. The best retrieval of the LW CERES surface (BOA) fluxes is
265 achieved using cloud properties derived from MODIS and processed to agree with observed LW
266 TOA fluxes (Gupta et al., 1992). They have been compared to other observations and validated
267 against surface radiation measurements (Gupta et al., 2010, Kratz et al., 2020) for mid and low
268 latitudes. In the Single Satellite Footprint (SSF) product Level2, adding MODIS cloud retrievals
269 and Goddard Meteorological Assimilation Office (GMAO) atmospheric profiles, the BOA fluxes
270 at the surface are also available in a 20 km x 20 km grid. CERES BOA fluxes are used as part of
271 the Arctic Observation and Reanalysis Integrated System (ArORIS) gathering several datasets
272 for climate studies in this region (Christensen et al., 2016). Initial comparisons over Greenland
273 showed small dispersion (Christensen et al., 2016) confirmed by further studies over the whole
274 Arctic (Huang et al., 2017b).

275
276 The CLOUDSAT-2B-FLXHR-LIDAR (hereafter named as C-C-FLX) products provide a
277 direct estimation of TOA and BOA fluxes consistent with the liquid and ice water content and
278 the cloud vertical profiles obtained from CloudSat, CALIOP and MODIS measurements, using
279 atmospheric profiles from ECMWF (Henderson et al., 2013, L’Ecuyer et al., 2008). The TOA
280 and BOA flux amount are defined as the first and the last non-zero value of FU and FD
281 parameters in the last available version product (R05) presently used from the CloudSat data
282 center (<http://www.cloudsat.cira.colostate.edu/data-products/level-2b/>). In this study we use the
283 currently available R05 products (<http://www.cloudsat.cira.colostate.edu/data-products/level-2b/2b-flxhr-lidar>), publicly available since March 2020, and discuss differences with previous
284 version R04. As the CLOUDSAT-2B-FLXHR-LIDAR R05 product is expected be less prone to
285 atmospheric biases due to cloud phase, well identified by lidar (Hu et al., 2009), we considered it
286 to better represent clouds in flux calculations.

287
288 The C-C-FLX (R05) time series starts in June 2006 and ends in August 2010 (April 2011
289 for R04) while CERES on AQUA begins in July 2002. Both products are expected to differ due
290 to factors related to cloud vertical distribution (Matus and L’Ecuyer, 2017). Whereas CERES is
291 based on MODIS data inversion, C-C-FLX input is a direct retrieval of vertical profiles from
292 CloudSat and CALIPSO active sensors. The cloud profiles are usually better constrained with
293 active instruments, even if some biases remain (Chan and Comiso, 2010). Moreover, it has been
294 shown that C-C misses some low clouds (B14). A second issue may be due to the spatial
295 distribution as C-C-FLX fluxes are given at the radar footprints (1.4 km) along a track whereas
296 the CERES grid is 20 km x 20 km, somewhat smoothing spatial variability. For both datasets, we
297 will discuss in sections 4.1.1 and 4.2.1 the representativeness of taking the nearest pixels to the
298 station versus an average of all the values located at less than 25 km from the station.

300

301 2.3 Fluxes from re-analysis

302 The ECMWF ERA-Interim (hereafter ERA-I) project is based on meteorological
 303 reanalysis that were assimilated from various datasets (Dee et al., 2011). ECMWF Integrated
 304 Forecast System uses a four-dimensional variational data assimilation (4DVar). In this study, we
 305 considered monthly average from a $0.125^\circ \times 0.125^\circ$ grid interpolated from the original 80 km x
 306 80 km special resolution, which represents approximately 14 km x 2 km at the latitude of Eureka.
 307 For coincident comparison purposes, ECMWF's ERA-I 3-hour reanalysis products were used,
 308 which corresponds to a delay of 60 and 45 minutes with A-Train overpasses near 11:00 and
 309 15:45 UTC respectively. The ECMWF most advanced reanalysis product, ERA5, was recently
 310 released and provides several improvements compared to ERA-I, as detailed by Hersbach and
 311 Dee (2016), and uses a more advanced 4DVar assimilation scheme, and higher vertical (137 vs.
 312 60 levels) and horizontal resolutions (31 km vs. 79 km).

313

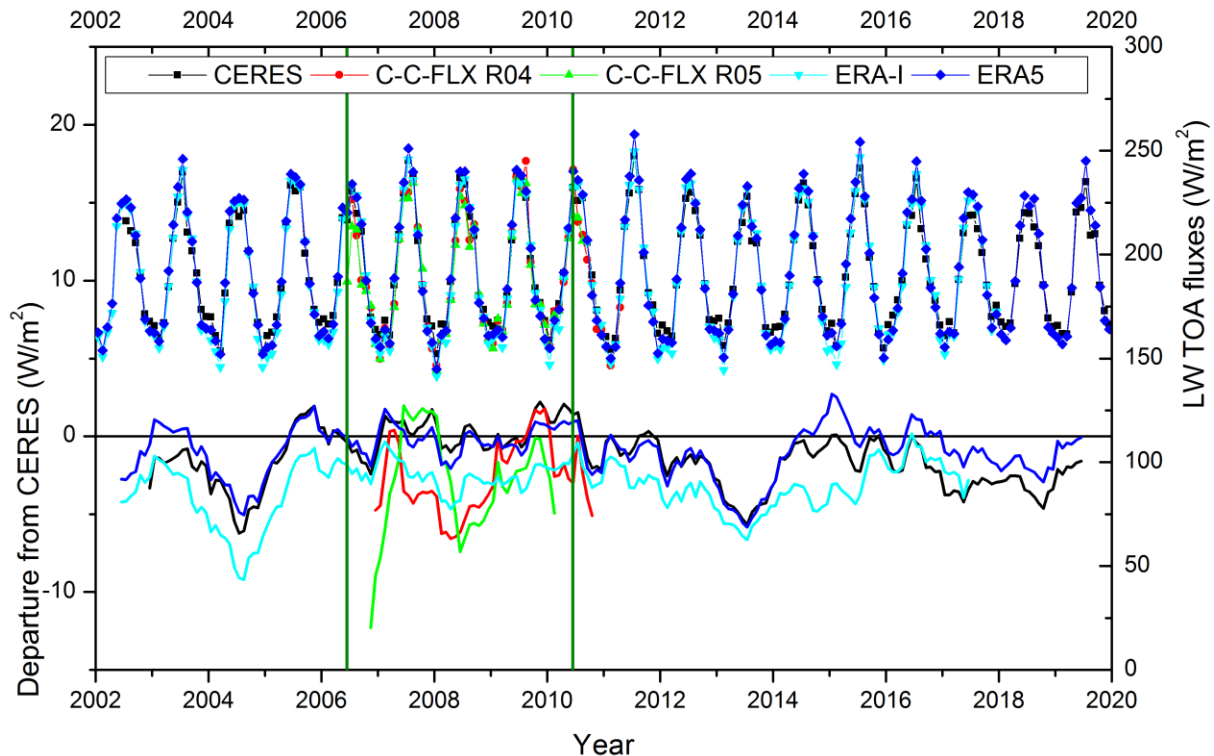
314 **3 Statistics from independent datasets**

315 In this section, as well as in the next section dealing with coincident measurements, we
 316 will first analyze TOA LW fluxes followed by downwelling fluxes at the surface.

317 3.1 TOA fluxes

318 LW TOA monthly fluxes from CERES observations, CALIPSO-CloudSat flux
 319 calculations and reanalysis from ERA5 are shown in Figure 2 for a period which extends from
 320 2002 to 2020.

321



322

323 **Figure 2.** Monthly variation of TOA LW fluxes (right side scale) measured and derived from
 324 satellite (CERES in black and CloudSat-2B-FLXHR-LIDAR R04 (in red), R05 (in green) and re-

325 analysis (ERA-I in cyan and ERA5 in blue) at Eureka from 2002 to 2020. 12-month moving
 326 average departures (left hand scale) from 2006/06-2010/05 CERES average are shown in the
 327 bottommost graph. The common observation period of this study is bounded by vertical green
 328 lines.

329
 330 Monthly variations are similar amongst the datasets, minimum values being observed in
 331 winter and maximum values in summer, with the range of the annual cycle being about 70-80
 332 W/m^2 , depending on dataset. ERA5 and CERES are available over the full period from 2002 to
 333 2020, whereas C-C-FLX R05 are limited to a period of 4 years (5 years for R04), as mentioned
 334 in the previous section. Plots in the lower graph of Figure 2 show the departure of 12-month
 335 moving average for each dataset from CERES 2006-2010 multi-year mean, which is the common
 336 observation period. It is seen that C-C-FLX R05 data are biased low on average by about 5 W/m^2
 337 as compared to CERES data. R04 shows similar values except the low values at the end of 2006.
 338 Two periods (respectively 2004 and 2013) in the whole CERES and ERA sequence were
 339 significantly different from the 2006-2010 average with departure larger than the overall
 340 standard deviation of 2.0 W/m^2 . More particularly, those periods show values comparable to or
 341 larger than 3 times the standard deviation. They occurred before and after the reference period in
 342 2004 and 2013 for both CERES and ERA5 datasets. Note that the 12-month moving average
 343 from ERA5 are generally in good agreement with those from CERES, except a small difference
 344 of about -2 W/m^2 since 2014. R05 data show significant differences and appear to be biased low
 345 with respect to CERES and ERA5.

346
 347 Average values, seasonal variations, trends and standard deviations are reported in Table
 348 2 for both 18 and 4-year periods. Departures from CERES, considered here as the reference for
 349 TOA LW fluxes, are shown in the second part of Table 2. ERA-I statistics are also included to be
 350 discussed along with newly available ERA5.

351
 352 **Table 2.** Annual and seasonal variations of LW TOA fluxes for CERES, C-C-FLX (R04 and
 353 R05), ERA-I and ERA5 over the whole dataset period and coincident period (July 2006 to May
 354 2010) based on monthly means. Linear trends are bolded when considered significant (more than
 355 2 sigma). Colour shading is representative of the difference with the reference (red when they are
 356 above CERES (darker) by more than 5 W/m^2 , blue below, green is within 2 W/m^2)

TOA	Time period	Annual mean		DJF		MAM		JJA		SON		ONDJFM	
		Mean (σ)	Trend (W/m^2 / year)	Mean (σ)	Trend (W/m^2 / year)	Mean (σ)	Trend (W/m^2 / year)	Mean (σ)	Trend (W/m^2 / year)	Mean (σ)	Trend (W/m^2 / year)	Mean (σ)	Trend (W/m^2 / year)
STATISTICAL ANALYSIS OVER THE WHOLE OBSERVATION PERIOD													
CERES	07/2002 - 12/2019	191.2 (2.0)	-0.1 (0.1)	164.3 (2.8)	0.1 (0.1)	187.6 (3.0)	0.1 (0.2)	226.3 (6.6)	-0.5 (0.3)	186.9 (2.0)	-0.1 (0.1)	169.3 (1.8)	0.0 (0.1)
C-C-FLX R04	07/2006 - 04/2011	189.4 (2.4)	0.8 (1.2)	158.5 (4.8)	0.8 (1.7)	184.0 (4.0)	3.0 (0.6)	226.4 (8.5)	1.5 (3.0)	184.7 (2.8)	-0.4 (1.0)	165.6 (3.2)	0.3 (1.1)

C-C-FLX R05	06/ 2006 - 08/ 2010	190.7 (4.0)	-0.1 (2.2)	158.3 (5.5)	3.2 (2.0)	183.4 (4.5)	3.2 (1.0)	220.0 (11.8)	2.4 (4.1)	188.4 (10.1)	-1.2 (5.4)	165.9 (2.5)	1.7 (0.6)
ERA-I	01/ 2002 - 12/ 2017	189.4 (2.0)	0.1 (0.1)	155.9 (3.0)	-0.1 (0.2)	184.6 (2.9)	0.3 (0.1)	229.9 (4.7)	0.1 (0.3)	187.0 (2.5)	0.0 (0.1)	163.5 (2.4)	0.1 (0.1)
ERA5	01/ 2002 - 12/ 2019	191.7 (1.8)	0.0 (0.1)	159.2 (2.7)	0.0 (0.1)	189.2 (3.0)	0.1 (0.1)	232.5 (5.8)	0.0 (0.3)	185.8 (2.6)	-0.1 (0.1)	165.1 (2.1)	0.0 (0.1)
STATISTICAL ANALYSIS OVER THE COMMON OBSERVATION PERIOD													
	Time period	Annual mean		DJF		MAM		JJA		SON		ONDJFM	
		Mean (σ)	Minus CERES	Mean (σ)	Minus CERES	Mean (σ)	Minus CERES	Mean (σ)	Minus CERES	Mean (σ)	Minus CERES	Mean (σ)	Minus CERES
CERES	06/ 2006 - 05/ 2010	192.7 (2.1)		164.8 (2.5)		187.7 (4.5)		230.7 (6.4)		187.4 (1.1)		169.5 (2.3)	
C-C-FLX R04	06/ 2006 - 05/ 2010	188.8 (4.3)	-3.8 (2.5)	159.3 (5.1)	-5.6 (3.1)	184.0 (4.0)	-3.7 (3.3)	227.4 (9.4)	-4.0 (5.9)	185.2 (2.9)	-2.2 (3.4)	166.1 (3.4)	-3.4 (1.2)
C-C-FLX R05	06/ 2006 - 05/ 2010	188.6 (6.2)	-5.4 (3.2)	158.3 (5.5)	-6.1 (2.7)	183.4 (4.5)	-4.3 (3.2)	221.4 (13.1)	-9.3 (7.5)	188.4 (10.1)	-1.3 (6.2)	165.9 (2.5)	-3.6 (0.5)
ERA-I	06/ 2006 - 05/ 2010	190.1 (0.6)	-2.6 (1.5)	156.4 (3.1)	-8.4 (1.1)	184.1 (2.6)	-3.6 (2.1)	231.9 (4.5)	1.2 (2.4)	187.9 (2.5)	0.5 (1.6)	163.3 (1.8)	-6.1 (1.4)
ERA5	06/ 2006 - 05/ 2010	192.3 (1.2)	-0.4 (0.9)	159.3 (3.3)	-5.5 (0.9)	188.7 (3.1)	1.0 (1.5)	234.9 (6.1)	4.2 (1.0)	186.2 (2.5)	-1.2 (1.5)	165.0 (2.2)	-4.4 (1.1)

357

358

359

360

361

362

363

364

365

366

367

Table 2 shows that it is also the case during the selected intensive common observation period, where both C-C-FLX releases are about 5 W/m² smaller than CERES in winter and less than 4 W/m² the rest of the seasons. The difference of 5.3 W/m² in JJA between C-C-FLX R04 and R05 may be explained by more data available in R05 in 2006 summer, but also by the longwave land emissivity that varies by surface type in R05 (Henderson and L'Ecuyer, 2020). While C-C-FLX is always smaller than CERES. The statistics over the whole observation period show that ERA-I has slightly smaller TOA LW fluxes than CERES but that ERA5 are similar to CERES and closer on the annual means. Both ERA datasets are close to CERES, except in winter where they are closer to C-C-FLX showing an 8.4 W/m² and 5.5 W/m² deficit relative to CERES. The use of ERA5 over ERA-I (with developments in model physics, core dynamics,

368 assimilation system, higher spatial and temporal resolution) leads to an increase in LW fluxes by
369 several W/m^2 and significantly reduces the bias with CERES, except in summer where the bias is
370 increased. Autumn shows the opposite behaviour with decreased fluxes in ERA5, and degraded
371 agreement. Note that the warm ground temperature bias in ERA reanalyses (Wang et al., 2019) is
372 not relevant in our study because weather observations at Eureka are assimilated.

373

374 CERES, ERA-I and ERA5 do not show significant trends in LW TOA fluxes in the last
375 eighteen years, neither on average nor on a seasonal analysis. The trends are significant only for
376 C-C-FLX dataset in spring when trend is larger than 2 sigma. C-C-FLX annual data show a
377 much larger variability between 2006 and 2010, as compared to the three other datasets that have
378 a larger footprint.

379

380 To summarize, TOA averages over the whole periods appear to be in good agreement for
381 all datasets (within about $5 \text{ W}/\text{m}^2$). Only small differences (CERES can be larger by about 6 to 8
382 W/m^2 than C-C-FLX, ERA5 and ERA-I in DJF) are observed on seasonal TOA fluxes, and these
383 differences are consistent with previous work (Loeb et al., 2018).

384 3.2 BOA fluxes

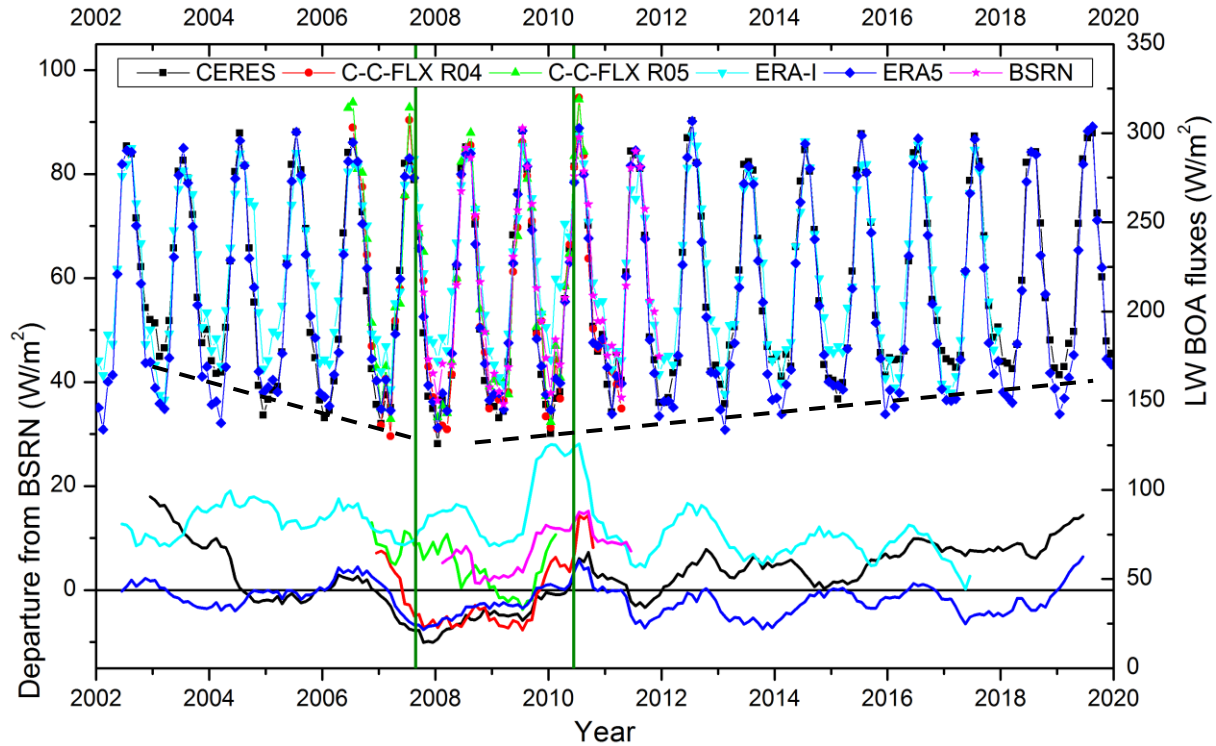
385 Figure 3 presents the comparison of the LW BOA downwelling fluxes from CERES,
386 ERA-I and ERA5 over the full 2002-2020 period, and along with the C-C-FLX, the reference
387 ground-based broad-band radiation dataset over a more restricted period of time. Table 3 gives
388 the yearly and seasonal average values as well as the estimated trends.

389

390 Note that the screening method described in section 2.1 and Appendix A helps to remove
391 suspicious measurements (184572 cases representing about 8% of the whole dataset). But this
392 filtering resulted in an under-representation of clear sky and then higher seasonal LW (up to 2.8
393 W/m^2 in winter, see Table 3). Therefore, those values are not expected to be used for
394 climatological analysis, but as a point of comparison with other datasets.

395

396



397
 398 **Figure 3.** Monthly variation of BOA LW fluxes (right side scale) measured and derived from the
 399 ground (filtered BSRN), from satellite (CERES and CloudSat-2B-FLXHR-LIDAR R04 and
 400 R05) and re-analysis (ERA-I and ERA5) at Eureka from 2002 to 2020. Black dashed lines
 401 represent estimated trends on CERES annual minimum. 12-month moving average departures
 402 (left hand scale) from 2007/09-2010/05 BSRN average are shown in the bottommost graph. The
 403 common observation period of this study is bounded by vertical green lines.
 404

405 Figure 3 shows a good agreement between all LW BOA fluxes for the summer, where
 406 annual cycle maxima among datasets vary within 5 W/m^2 , except for C-C-FLX R05 between
 407 2006 and 2010, where it exceeds 20 W/m^2 . Large differences between the datasets are observable
 408 in winter with divergence at minimum as large as 30 W/m^2 in 2003. Variation of winter fluxes
 409 for CERES shows a V-shape trend (see Fig. 3). The average decrease is about 30 W/m^2 from
 410 2002 to the middle of the period analyzed e.g. between 2008 and 2009, and an increase after
 411 (representing about 20 W/m^2). This increase in CERES fluxes may be due to the increase in low
 412 cloud winter temperature or changes in low cloud fraction over this part of the Arctic. This trend
 413 is however not seen on ERA5 (and ERA-I) datasets as was evidenced in meteorological trends
 414 observed in Arctic (Jun et al., 2016, Graham et al., 2019a). This V-shape trend observed in
 415 winter over the 18-year period tends to reduce the overall trend as reported in Table 3. Some
 416 residual low frequency (about 10 years) modulation is apparent, in particular during the winter
 417 months, with a small peak-to-peak amplitude (about 3 W/m^2). BSRN data tend to agree with the
 418 uniformity of LW BOA fluxes measured in summer at Eureka (standard deviation of 1.8 W/m^2
 419 between 2007 and 2011, see Table 3), and the low values ($\sim 165 \text{ W/m}^2$) measured in the winters
 420 from 2008 to 2010.
 421

422 From Table 3 (see also Fig. 3), it is seen that CERES statistics over the 18-year period is
 423 about 5 W/m² smaller than BSRN averages, but over the common period, this difference
 424 increases to up to 10 W/m². C-C-FLX is also smaller over this period but R05 shows reduced
 425 bias in all seasons compared to R04. Major changes were made in C-C-FLX R05 to improve the
 426 representation of cloud properties (cloud detection, supercooled liquid and ice clouds
 427 microphysical properties) along with updated data ingested. The annual difference is still lower
 428 than BSRN by 2.4 W/m² over the common observation period and is mainly attributed to
 429 differences observed in winter (DJF) when differences are about 10 W/m², consistent with the
 430 aforementioned sampling limitations in the BSRN during the icing season. C-C-FLX R04 shows
 431 higher bias during the polar night (ONDJFM) with peak differences being observed between C-
 432 C-FLX R04 and BSRN in winter that reach -17.3 W/m².

433
 434 The reanalysis averages reported in Table 3 show interesting features with a correction of
 435 fluxes in ERA5, that reduces annual fluxes by 14 W/m² on average with respect to ERA-I. This
 436 reduction in LW downwelling fluxes occurs almost all year, except in June and July. As for TOA
 437 comparison, several reasons could explain the better performance of ERA5, e.g. a more detailed
 438 data assimilation system with higher vertical resolution and better surface and radiation models.
 439 Although ERA5 is closer to BSRN than ERA-I, it still underestimates LW BOA by ~15 W/m² in
 440 ONDJFM, relatively to BSRN measurements. As seen from Fig. 3, ERA5 and BSRN are in good
 441 agreement over the period of minimal winter fluxes, but although in good agreement with
 442 CERES in summer, ERA5 does not show winter flux increases seen by CERES.

443
 444 **Table 3.** Annual and seasonal variations of LW BOA fluxes for CERES, C-C-FLX (R04 and
 445 R05), ERA-I, ERA5 and BSRN over the whole dataset period and coincident period (September
 446 2007 to May 2010) based on monthly means. Linear trends are bolded when considered
 447 significant (more than 2 sigma). Colors indicate differences with BSRN fluxes taken as a
 448 reference (orange when they are above BSRN by more than 2 W/m², blue below -2 W/m², green
 449 in between). Darker colors are used above +/- 10 W/m²).

BOA	Time period	Annual mean		DJF		MAM		JJA		SON		ONDJFM	
		Mean (σ)	Trend (W/m ² / year)	Mean (σ)	Trend (W/m ² / year)	Mean (σ)	Trend (W/m ² / year)	Mean (σ)	Trend (W/m ² / year)	Mean (σ)	Trend (W/m ² / year)	Mean (σ)	Trend (W/m ² / year)
STATISTICAL ANALYSIS OVER THE WHOLE OBSERVATION PERIOD													
	09/ 2007 - 12/ 2011	216.1 (3.7)	1.0 (1.9)	168.9 (11.0)	7.7 (2.6)	189.5 (10.0)	-1.5 (5.4)	282.4 (1.8)	1.0 (0.7)	219.0 (4.9)	2.3 (1.2)	178.9 (7.6)	5.4 (1.8)
unfiltered	09/ 2007 - 12/ 2011	214.8 (3.7)	0.6 (2.0)	166.1 (8.4)	5.9 (2.0)	188.8 (10.0)	-2.0 (5.3)	282.4 (1.8)	1.0 (0.7)	217.2 (5.0)	2.5 (1.1)	176.2 (6.5)	4.5 (1.6)
C-C-FLX R04	07/ 2006 - 04/ 2011	205.9 (6.5)	3.0 (2.8)	152.7 (12.8)	6.0 (3.2)	182.0 (12.9)	6.9 (5.1)	286.0 (9.2)	-0.3 (3.4)	211.0 (10.1)	-5.5 (2.0)	165.1 (7.1)	2.2 (2.3)

C-C-FLX R05	07/ 2006 - 08/ 2010	211.4 (7.0)	-6.6 (2.5)	155.5 (7.9)	0.4 (4.3)	185.8 (11.7)	6.6 (4.4)	289.9 (13.0)	-2.5 (4.5)	227.1 (12.7)	-8.6 (3.4)	171.2 (4.1)	-1.1 (2.1)
CERES	07/ 2002 - 12/ 2019	211.2 (6.1)	0.5 (0.3)	160.2 (14.5)	0.7 (0.7)	192.1 (7.1)	0.1 (0.4)	286.0 (4.4)	0.3 (0.2)	208.1 (8.1)	0.3 (0.4)	170.1 (12.1)	0.6 (0.6)
ERA-I	01/ 2002 - 12/ 2017	220.0 (6.0)	-0.4 (0.3)	174.9 (9.3)	-0.9 (0.5)	201.4 (10.8)	-0.2 (0.6)	279.4 (5.2)	0.1 (0.3)	224.4 (7.8)	-1.1 (0.3)	186.8 (7.6)	-0.7 (0.4)
ERA5	01/ 2002 - 12/ 2019	206.5 (3.6)	0.0 (0.2)	153.5 (5.4)	-0.2 (0.3)	185.0 (4.7)	0.1 (0.2)	284.1 (4.9)	0.1 (0.2)	203.6 (6.6)	-0.1 (0.3)	164.0 (4.2)	-0.1 (0.2)
STATISTICAL ANALYSIS OVER THE COMMON OBSERVATION PERIOD													
		Annual mean		DJF		MAM		JJA		SON		ONDJFM	
	Time period	Mean (σ)	Minus BSRN	Mean (σ)	Minus BSRN	Mean (σ)	Minus BSRN	Mean (σ)	Minus BSRN	Mean (σ)	Minus BSRN	Mean (σ)	Minus BSRN
filtered	09/ 2007 - 05/ 2010	205.8 (16.2)		163.9 (6.1)		192.4 (10.0)		280.9 (1.1)		217.5 (6.4)		175.8 (5.2)	
BSRN unfiltered	09/ 2007 - 05/ 2010	204.7 (16.1)	-1.1 (0.2)	162.5 (5.4)	-1.4 (0.7)	192.0 (9.4)	-0.4 (0.7)	280.9 (1.1)	0.0 (0.0)	215.3 (6.1)	-2.2 (0.6)	173.6 (4.7)	-2.1 (0.6)
C-C-FLX R04	09/ 2007 - 05/ 2010	195.9 (18.7)	-8.3 (2.2)	146.6 (5.3)	-17.3 (6.8)	183.0 (15.7)	-3.1 (3.1)	279.5 (9.7)	-1.4 (8.7)	209.4 (2.1)	-8.2 (7.0)	160.7 (3.4)	-13.5 (3.9)
C-C-FLX R05	09/ 2007 - 05/ 2010	203.1 (15.2)	-2.4 (4.4)	153.7 (8.5)	-9.7 (9.3)	187.1 (14.0)	0.4 (2.4)	281.1 (15.3)	0.2 (14.2)	223.6 (13.1)	-0.1 (8.7)	169.5 (3.0)	-4.7 (5.6)
CERES	09/ 2007 - 05/ 2010	193.9 (20.0)	-10.8 (4.0)	142.8 (2.1)	-21.2 (6.3)	187.8 (10.5)	0.8 (3.8)	284.9 (3.3)	4.0 (2.3)	198.2 (3.6)	-19.3 (2.9)	154.1 (2.6)	-21.3 (4.2)
ERA-I	09/ 2007 - 05/ 2010	218.6 (15.1)	13.8 (5.9)	181.6 (12.0)	17.6 (6.1)	212.6 (21.0)	25.4 (12.5)	279.3 (4.4)	-1.6 (3.3)	225.9 (4.4)	8.4 (2.3)	191.1 (11.4)	16.0 (6.0)
ERA5	09/ 2007 - 05/ 2010	196.4 (18.4)	-8.1 (2.7)	150.8 (4.0)	-13.2 (5.9)	188.3 (8.2)	2.2 (6.9)	283.8 (1.3)	2.9 (0.2)	198.9 (1.6)	-18.6 (4.8)	159.9 (3.1)	-15.1 (4.2)

450

451 As a first conclusion on these seasonal average analysis of BOA fluxes (Table 3), CERES
452 and C-C-FLX averages derived from space observations and ERA5 reanalysis are in rather good
453 agreement although about 10 W/m^2 smaller than BSRN. They can even be larger than -20 W/m^2
454 during the polar night (ONDJFM). Conversely, ERA-I appears to be biased high with respect to
455 all observations except in JJA, where all results are in agreement within 4 W/m^2 . The observed
456 bias of ERA-I is coherent with previous analyses, where an over-estimation of low-cloud cover
457 causes higher LW BOA in winter, whereas ERA-I LW are subject to a dry bias in summer
458 (Zygmuntowska et al., 2012; Zib et al., 2012; Chernokulsky and Mokhov, 2012; Lenaerts et al.,
459 2017; Huang et al., 2017a). Although relatively few studies with ERA5 evaluation in the Arctic
460 are available, it seems that several biases of ERA-I are better addressed in ERA5, in terms of
461 representation of temperature and humidity profiles and wind speed near surface (Graham et al.,
462 2019a; Graham et al., 2019b; Betts et al., 2019). However it is not clear if low cloud fraction is
463 better represented.

464

465 In order to further analyze the origin of these differences, we come back to cloud vertical
466 information as it was identified in B14 as a source of difference in sensitivities.

467

468 3.3 Cloud vertical structure and type at Eureka

469 Over the June 2006 to May 2010 period, the number of vertical profiles was 329,204 for
470 EUR-LR (1 profile every 3 minutes), 57,976 for MODIS on AQUA (taking all the pixels whose
471 center is less than 25 km from Eureka), 16,927 for DARDAR (481 overpasses; this dataset,
472 DARDAR-MASK-v1.1.4 is based on CloudSat and CALIPSO synergy, as described in Delanoë
473 and Hogan, 2010 and Ceccaldi et al., 2013), 17,024 for CloudSat-CLDCLASS-LIDAR R05
474 (labelled as C-C in Fig.4) and 5,844 reanalyses for ERA-I and ERA5.

475

476 DARDAR, C-C and EUR-LR have similar vertical distributions of cloud layers above 3
477 km. As detailed in B14 and Liu et al. (2017), very low clouds are difficult to address from space,
478 and this is confirmed here from DARDAR, C-C and MODIS for which cloud fractions are much
479 lower than EUR-LR ground-based observations below 2 km, as evidenced in Fig. 4. Compared
480 to EUR-LR, DARDAR and C-C are close in all seasons, except for high clouds ($z > 8 \text{ km}$) in
481 autumn and winter (that may be due to the use of a better vertical resolution in DARDAR, which
482 is sampled at CALIOP vertical resolution). DARDAR and C-C give close results although
483 DARDAR gives a higher amount of ice clouds and less mixed-phase clouds (see Appendix B).
484 We find that the cloud fraction in reanalysis is generally biased low below 8 km, which is
485 consistent with the findings of Liu and Key (2016) for a larger region of the Arctic.

486

487 In general, there is good agreement in the vertical profiles of cloud fraction excepting
488 MODIS, ERA5 and ERA-I, which are systematically smaller than the other datasets (and this is
489 particularly the case for ERA5). In spring, although slightly smaller than ground-based
490 observations, cloud fractions from all sources agree above 5 km, but significant discrepancies are
491 observed below this altitude and even more below 2 km, in agreement with previous findings
492 from B14.

493

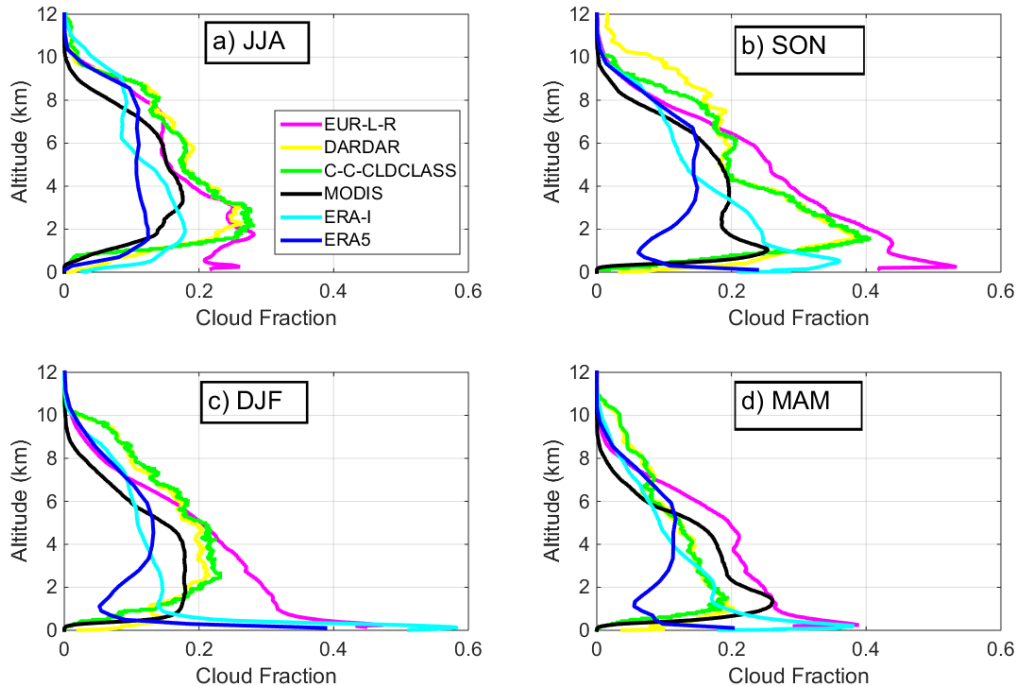


Figure 4. Cumulated seasonal vertical scene-type distribution between June 2006 and May 2010 all the independent datasets at less than 25 km from the station.

Low clouds detected by EUR-LR are more frequent in all seasons but summer (JJA), especially in winter (DJF) when the difference with the other datasets is larger (Fig. 4). An occurrence peak is observed by EUR-LR near the surface (within the first 500 to 1000 m) during winter (and spring), only captured by ERA5 and ERA-I. MODIS strongly underestimates low clouds in summer, and, to a lesser extent, in other seasons. B14 also showed that MODIS underestimates cloud fraction during winter (from October to February). This is a known issue (Liu et al., 2010). MODIS cloud fraction biases vary with season, as the complete darkness during the polar night prevents the use of visible channels for cloud retrievals and implies the use of a nighttime cloud detection algorithm (Liu et al., 2004). MODIS distribution peaks at 1km in MAM, when the temperature inversion is the strongest, about 10°C on average. ERA-I misses mid and high clouds in all seasons with a large increase in the near surface cloud fraction from September to May. This was also discussed by Zygmuntowska et al., 2012 and Zib et al., 2012). ERA5 better captures mid- and high-level clouds, which are mainly ice clouds, but largely misses low clouds at SON, DJF and MAM, especially above 500 to 1000m, where near-surface temperature inversion usually occurs.

In DJF, satellite observations and analyses dramatically lack low level clouds (between 0 and 4 km), where most of Arctic clouds occur (Shupe et al., 2011a). This is compensated in ERA-I and ERA5 by an excess of near surface clouds. In all seasons DARDAR, C-C and MODIS lack low clouds below 1 km. Spaceborne radar detection suffers from surface contamination echo, and lidar detection efficiency is decreased by attenuation in liquid water clouds. In most seasons, EUR-LR is missing some high clouds, due to the attenuation of lidar signal in opaque clouds and due to decreasing radar sensitivity with range. The better agreement (above 7 km) is obtained in JJA and the larger dispersion in this altitude range is observed in SON.

523

524 Large differences in BOA fluxes, in Table 3, were observed during winter, which is the
 525 period when significant mismatch appears in cloud vertical distribution. This deficit of low
 526 clouds lowers BOA fluxes calculated from satellite dataset, compared to BSRN. The smaller
 527 contribution of MODIS low clouds at this season can explain the lower LW BOA value of
 528 CERES compared to C-C-FLX. This is the opposite for MAM. The excess of near surface
 529 clouds for ERA5 (and to a lower extent for ERA-I) in DJF and MAM, combined with a warmer
 530 temperature profile compared to radiosondes (not shown), can also explain the over-estimation
 531 of downwelling fluxes for ERA5 (and ERA-I).

532

533 To go further in the comparison of fluxes, we looked to coincident datasets following the
 534 B14 approach.

535 4 Coincident measurements from independent datasets

536 In this section we will focus on TOA and BOA flux analyses for the subsets of coincident
 537 observations in space and time. We consider here the datasets that directly provide radiative
 538 fluxes (CERES and C-C-FLX) and datasets for which we have calculated fluxes (EUR-LR)
 539 using Streamer RTM. Note that ERA-I and ERA5 data points are not strictly coincident with A-
 540 Train overpasses, but as they are within approximately 1 hour, we included them in the analysis.
 541 For TOA we compared all datasets CERES, C-C-FLX, EUR-LR, ERA-I and ERA5 keeping
 542 CERES as a reference, whereas for BOA, the same datasets were considered with BSRN acting
 543 as the reference.

544 4.1 TOA fluxes

545 4.1.1 Mean seasonal TOA fluxes

546 Here, we will analyze the evolution of seasonal fluxes at TOA for the different datasets
 547 with respect to CERES and discuss correlations and histograms of spread. We will further study
 548 differences by type of scene. This analysis includes 249 coincident samples, seasonally
 549 distributed as DJF=56; MAM=67; JJA=47; SON=79. Mean seasonal fluxes from coincident
 550 measurements highlights any systematic bias between datasets. Table 3 summarizes the average
 551 values determined for all the seasons and annual mean.

552

553 **Table 4.** Seasonal LW TOA average fluxes for coincident CERES and other retrievals for the
 554 period spanning from 09/2006 to 04/2010. C-C-FLX R05 is put aside at the end of the table due
 555 to smaller data points compared. Standard deviations are in brackets. Colors are reported as in
 556 Table 2.

TOA	Total		DJF		MAM		JJA		SON	
# of cases	249		56		67		47		79	
	Mean (σ)	Minus CERES 25 km								
CERES < 25km	192.1 (30.4)		164.0 (13.1)		189.7 (21.5)		239.9 (16.1)		185.6 (16.9)	
CERES nearest	192.2 (30.6)	0.1	163.7 (13.5)	-0.2	189.9 (21.6)	0.2	239.9 (17.0)	0.0	185.8 (16.9)	0.3
EUR-LR	191.1	-1.0	163.6	-0.4	187.2	-2.5	237.1	-2.8	186.6	1.0

	(31.4)		(16.7)		(21.0)		(19.2)		(22.1)	
C-C-FLX R04 < 25km	188.3 (31.4)	-3.8	158.7 (12.6)	-5.3	187.4 (22.5)	-2.2	237.8 (14.4)	-2.2	180.5 (17.4)	-5.1
C-C-FLX R04 nearest	187.9 (32.3)	-4.1	156.9 (13.1)	-7.1	186.8 (22.9)	-2.8	238.4 (16.0)	-1.5	180.9 (18.1)	-4.6
ERA-I	187.4 (32.0)	-4.7	156.9 (15.4)	-7.1	183.8 (24.3)	-5.9	237.2 (12.1)	-2.7	182.4 (17.2)	-3.2
ERA5	191.3 (34.7)	-0.7	160.1 (13.7)	-3.8	191.5 (24.5)	1.8	246.2 (14.5)	6.3	180.6 (20.6)	-4.9
# of cases										
	221		46		65		47		63	
	Mean (σ)	Minus CERES 25 km								
C-C-FLX R05 < 25km	189.2 (31.4)	-5.2	157.3 (14.0)	-6.3	186.1 (22.2)	-3.6	234.6 (14.6)	-5.3	181.8 (17.5)	-6.0
C-C-FLX R05 nearest	188.5 (32.9)	-5.9	154.7 (15.0)	-8.8	185.3 (23.1)	-4.4	235.8 (16.5)	-4.1	181.1 (17.8)	-6.7

557

558

559 Table 4 allows for clarification of conclusions drawn from Table 2. There is a good
560 agreement between all datasets within 5 W/m^2 for annual LW TOA, with values in general larger
561 for CERES, the bias being higher during wintertime and, to a lesser extent, in autumn. Streamer
562 calculations, based on EUR-LR retrievals, agree well with CERES, except in spring and summer,
563 where they are smaller (but by less than 3 W/m^2). C-C-FLX R05 shows larger deficit than R04 in
564 all seasons with a total bias of -5.9 W/m^2 . Several changes in R05 could explain the difference
565 with R04, namely longwave land emissivity and cloud properties (Henderson and L'Ecuyer,
566 2020).

566

567 We propose to take a closer look at those differences in terms of seasonal differences,
568 depending on key parameters.

569

4.1.2 Seasonal flux differences and spatial heterogeneity

570

571 To assess the role of spatial heterogeneity, we compared the nearest and 25km circle-
572 mean value of each coincident measurement from CERES and C-C-FLX. Figure 5 displays LW
573 TOA departures from CERES ($< 25 \text{ km}$) as reported in Table 4. It shows a systematic
574 underestimation (mean annual bias of -3.1 W/m^2 with a standard deviation of 2.1 W/m^2) of LW
575 for all datasets compared to CERES. Part of this difference could be explained by the spatial
576 sampling over an heterogeneous and steep terrain (such as shown for Eureka in Fig. 1), where
577 surface temperatures are hard to precisely account for at the different pixel sizes among dataset
578 (CERES: $20 \times 20 \text{ km}$, C-C-FLX: 1 km , ERA: $14 \times 2 \text{ km}$). In winter this effect is expected to be
579 smaller because the region is ubiquitously snow and ice covered, limiting heterogeneity in
580 surface emissivity.

580

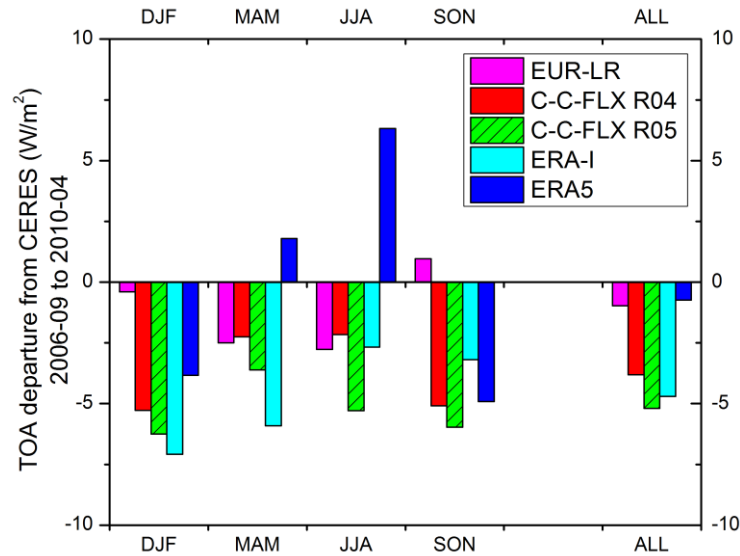
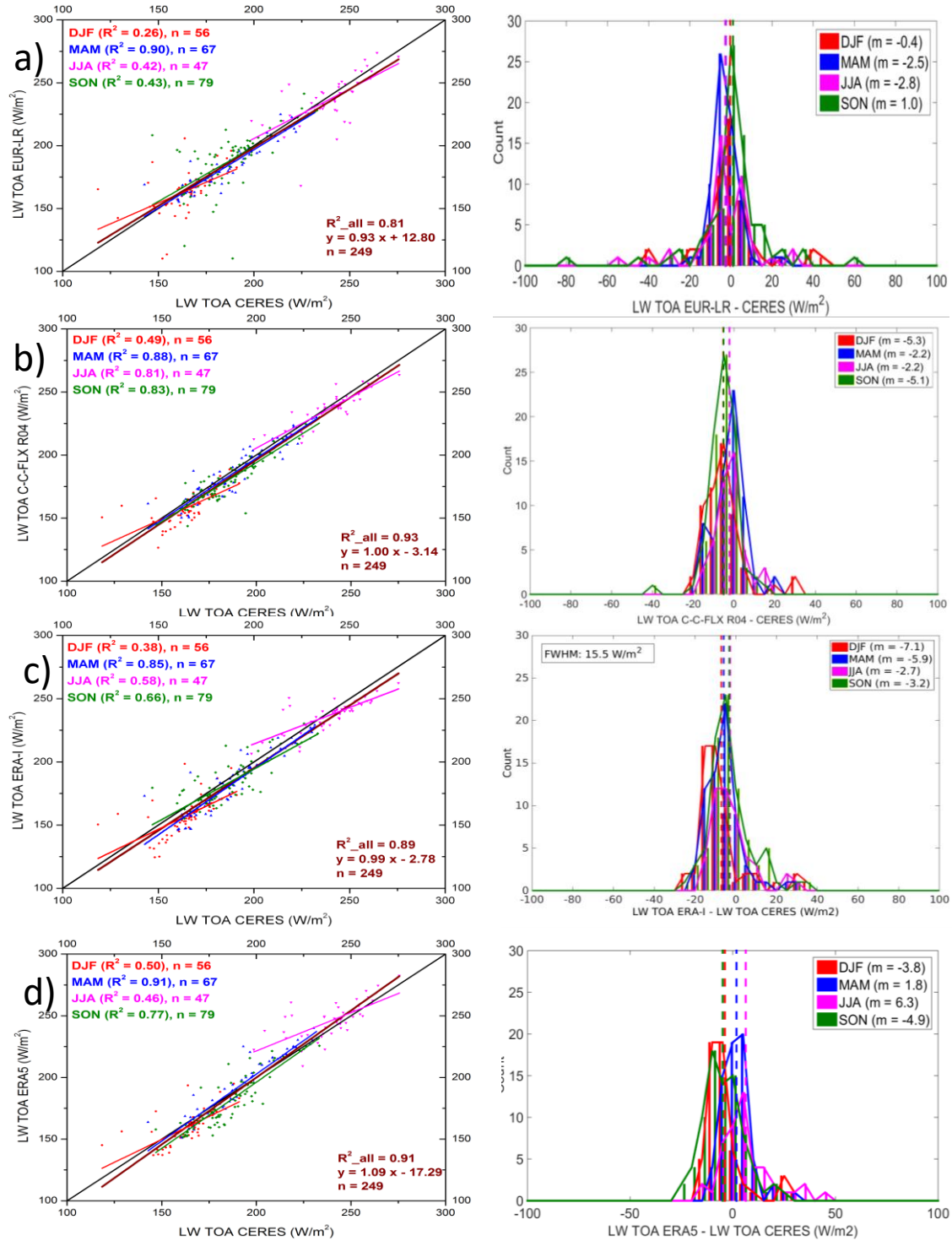


Figure 5. LW TOA departure from CERES as reported in Table 4. C-C-FLX R05 comparison with CERES is based on only 221 points (249 for R04 and other datasets).

Best agreement is seen from comparisons between CERES and the ground-based EUR-LR flux calculations with an absolute difference being maximum in MAM and JJA (about 2.5 W/m^2). Heterogeneity has a small impact for CERES (less than 0.3 W/m^2 because CERES measurements are to a certain extent smoothed in the $20 \times 20 \text{ km}$ pixel) and slightly higher for C-C-FLX (up to 1.8 W/m^2 for R04 and 2.5 W/m^2 for R05 in winter).

During this time of year, thick liquid and mixed-phase clouds obstruct higher clouds, from a ground-based perspective (Fig. 4). It further underscores the importance of the cloud vertical distribution in increasing accuracy of the radiative transfer calculations. As in Table 2, we see in Table 4 and Fig. 5 that the C-C-FLX and CERES differences are negative for all seasons. A good agreement is however obtained (about -3.8 W/m^2) between C-C-FLX and CERES. It is comparable to the one obtained in the statistical study although results for DJF and SON are degraded (see Fig. 6). Compared with Table 2, ERA5 bias with CERES is still small in average, but is degraded in summer and fall. This could be due to the temporal sampling of 3-hour re-analysis in seasons when atmospheric properties can rapidly change. ERA-I is behaving slightly differently with larger departures observed in DJF and MAM, consistently with Table 2. Overall the sampling effect does not appear as a first-order reason that can explain the differences in TOA between datasets.

Figure 6 shows scatter plots of the coincident retrieved LW TOA fluxes for EUR-LR, C-C-FLX R04, ERA-I and ERA5 and histograms of their differences with respect to CERES dataset. Note that C-C-FLX R05 plots are not shown here as the conclusions are similar to R04 and the number of points is smaller (see Table 5 where results are reported). In the scatter plots we have identified both seasonal and overall correlation coefficients. In the histograms and Table 5, we have identified the biases and half widths at 60% of the maximum and one fourth of the full width at $1/e^2$ of the maximum (e.g. one standard deviation - s - of a gaussian distribution), and the number of points outside $3s$ to give an indication of the outliers.



613
 614 **Figure 6.** Seasonal TOA upwelling LW fluxes for CERES and EUR-LR (a),
 615 C-C-FLX R04 (b),
 616 ERA-I (c) and ERA5 (d) for 249 measurements at the same time, between September 2006 and
 617 April 2011.

618 **Table 5.** Gaussian fit statistics of TOA differences between EUR-LR, C-C-FLX, ERA-I, ERA5
 619 and CERES. Note that a smaller number of points were available for R05 (see Table 4).

EUR-LR	C-C-FLX R04 -	C-C-FLX R05 -	ERA-I -	ERA5 -
--------	---------------	---------------	---------	--------

	- CERES	CERES	CERES	CERES	CERES
Mean	-1.3	-4.0	-5.6	-7.4	-2.7
Half width at 60%	7.0	6.8	6.3	7.3	8.7
FWHM	16.3	15.8	14.8	17.0	20.3
σ (¼ of full width at 1/e ²)	6.9	6.7	6.3	7.2	8.6
Number of outliers (> 3 σ)	26	5	5	14	8

620

621 Looking at EUR-LR plots and histograms, a few large seasonal outliers are evidenced in
 622 Fig. 6a and Fig. 6b, except in MAM which correspond to a smaller amount of high clouds (see
 623 Fig. 4). These outliers are homogeneously distributed below and above the mean. The worst
 624 correlations occurred in DJF, SON and JJA with differences up to 80 W/m² as one can see from
 625 the outliers of the histogram. In the case of opaque clouds, ground-based instruments are not able
 626 to correctly resolve the vertical profiles of cloud fraction, particle size and extinction at upper
 627 levels due to transmission losses. As a result, mean cloud temperature is set too high and this
 628 causes an overestimation of LW TOA. Another critical scenario is the presence of high clouds,
 629 sometimes above opaque clouds. Due to the decreasing radar sensitivity with range and the fact
 630 that the lidar signal can be totally attenuated in opaque clouds, it is likely to miss those high
 631 clouds and then underestimates LW TOA, with a bias that depends on cloud layer optical depth.

632

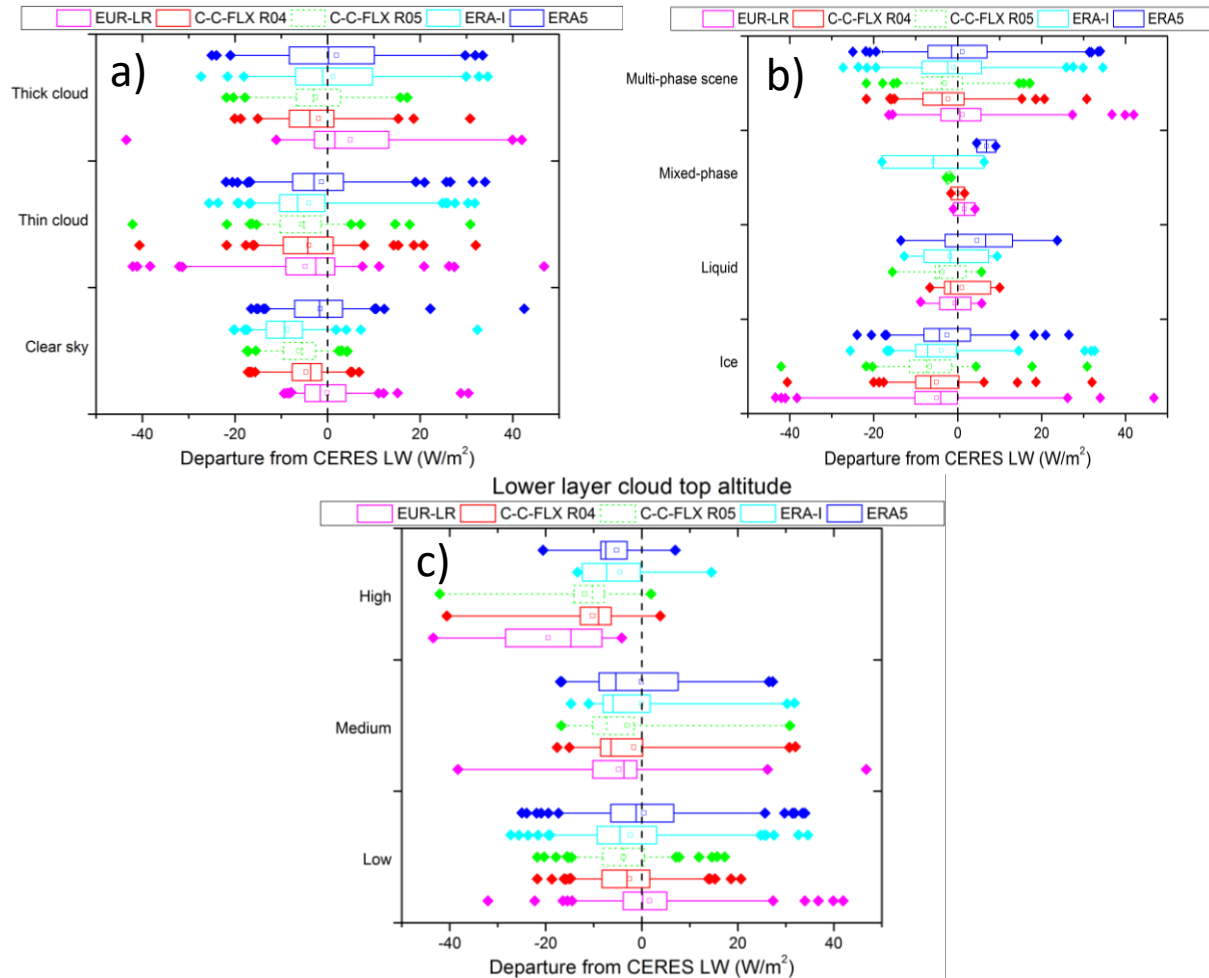
633 The good agreement noticed before between C-C-FLX R04 (and R05) and CERES
 634 corresponds to good correlation slopes but a higher dispersion with a weaker number of outliers
 635 than for EUR-LR. Differences are larger in winter (DJF) and in autumn (SON), where the slope
 636 is smaller than 1 and the outliers are more numerous, especially with large positives. In the
 637 histograms DJF and SON are indeed characterized by a larger bias with respect to CERES (about
 638 -5 W/m²). For these two seasons a rather broad dispersion is observed with a few outliers at +30
 639 W/m². In winter and spring, the difference shows a secondary peak at -10 W/m². This is not
 640 statistically significant, but it can be due to the under-estimation of low ice clouds, if one looks at
 641 cloud vertical fraction with respect to EUR-LR, but the overall number of points remains small
 642 for that to be significant.

643

644 ERA-I appears slightly biased low by about 7.4 W/m² on average, and the number of
 645 outliers is large. However their distribution is different from the EUR-LR one with a large
 646 number of positive values creating a secondary peak at +30W/m², not shown here. Finally, we
 647 find that ERA5 LW TOA is on average in relatively better agreement if we consider all points
 648 with a global correlation of R²=0.91, close to what is obtained for ERA-I. Seasonal scatter plot
 649 and histogram (Fig. 6d) highlight opposite pattern in winter and summer, with a much smaller
 650 correlation. It can be in part explained by the fact that ERA5 overestimates cloud cover
 651 (especially low cloud) in the Arctic in wintertime, in a way similar to (but less than) the one
 652 already shown for ERA-I (see Fig. 4), and consistent with previous work, done with ERA-I
 653 (Chernokulsky and Mokhov, 2012; Zyguntowska et al., 2012). The modest correlation in
 654 summer (R²=0.46) may be linked to the fact that ECMWF reanalyses underestimate by half the
 655 liquid water content of summer clouds (Zyguntowska et al., 2012; Huang et al., 2017a). This
 656 will be further discussed in the next subsection.

657 4.1.2 TOA differences decomposed by cloud optical depth, type of scenes and height of
 658 lower layer

659 To validate the hypothesis of section 4.1.2, that most differences are due to clouds, we
 660 now plot the LW differences depending on the total visible optical depth (Fig. 7a), the phase of
 661 cloud layers (Fig. 7b) and the top altitude of the lowest layer (Fig. 7c). We only keep ERA5 in
 662 these plots for sake of clarity, as showing comparable behavior, and will briefly discuss main
 663 differences with ERA-I. To compare with the same number of cases (249), only C-C-FLX-R04 is
 664 shown here but we discuss below the comparison between R04 and R05 with respect to CERES.
 665



666 **Figure 7.** Difference of TOA LW fluxes between DATASET (EUR-LR, C-C-FLX R04, R05,
 667 ERA-I and ERA5) minus CERES depending on (a) total visible optical depth, (b) phase of cloud
 668 layers and (c) top height of the lower layer. Boxes correspond to 25%, median and 75% values,
 669 thin bars show 5 and 95% and squares are used to show the mean. Outliers are also reported as
 670 coloured diamonds.
 671

672
 673 Note that the type of scene classification (either clear, thin or thick clouds), phase of
 674 clouds (liquid water, ice, mixed-phase or multiple phase scene) and top height of the lower layer
 675 are based on EUR-LR observations and therefore depends on instrument sensitivity and can be
 676 biased in the case of opaque clouds and very thin clouds. Thick/Thin clouds threshold is set to

677 total visible optical depth of 2. Multiple phase scene indicates that layers with different phase are
 678 present in the column.

679

680 Figure 7a confirms the relatively good agreement for TOA LW for clear-sky scenes. With
 681 a decreased departure from -8.7 to -2.6 W/m^2 , ERA5 reanalyses of clear sky are improved
 682 compared to ERA-I, where surface emissivity, surface temperature or atmospheric absorption
 683 have been identified as possible source of discrepancies, as shown in Huang et al. (2017a). The
 684 comparison between both C-C-FLX datasets shows degraded statistics for R05 relative to R04,
 685 especially for clear sky (median bias of -3.6 W/m^2 for R04 and -5.5 W/m^2 for R05). This could
 686 be due to changes in R05 implementation of longwave land emissivity, which is relatively
 687 complex to parametrize in heterogeneous and steep terrain like Eureka. There is a warm bias for
 688 EUR-LR due to the presence of thick clouds ($\text{COD} > 2$), when lidar signal is extinguished and the
 689 cloud layer top altitude is not precisely found. Therefore, the EUR-LR cloud layer are wrongly
 690 positioned (too low, too warm). TOA departures based on cloud type are fairly similar amongst
 691 datasets. EUR-LR fails to get correct LW TOA when high clouds are present, due to a decrease
 692 in radar sensitivity for small particles (as discussed in Grenier et al., 2009 and Blanchard et al.,
 693 2017).

694

695 Ice layers are very frequent and cause a large spread in TOA differences. There are very
 696 few liquid-phase clouds only (7) and mixed-phase only (2) cases. Figure 7c shows that all types
 697 of clouds are mainly biased low with respect to CERES TOA measurements, with an emphasis
 698 on high clouds. This is rather surprising for C-C-FLX R04 and R05, because of high sensitivity
 699 of lidar to cirrus clouds as evidenced in the high C-C-FLX cloud occurrence reported in Fig. 4. A
 700 possible reason could be inaccurate estimations of ice water content and microphysics in flux
 701 calculations, but this evaluation is beyond the scope of this study. It has also to be noted that
 702 some additional discrepancies could occur due to the temperature inversion layer which could be
 703 badly captured with GMAO or ERA5 coarse vertical resolutions.

704

705 Overall two main issues are confirmed here: the bias in high clouds for EUR-LR, and the
 706 bias in clear air identified for ERA-I is now corrected in ERA5.

707

708 4.2 BOA fluxes

709 4.2.1 Mean seasonal BOA fluxes

710 Between September 2007 and May 2010, both active instruments and BSRN sensor were
 711 operational at Eureka. Repeating the same methodology as in section 4.1, we first discussed
 712 annual and seasonal statistics.

713

714 **Table 6.** As for table 4, seasonal variation of LW BOA for BSRN, EUR-LR, CERES, C-C-FLX
 715 (R04 and R05), ERA-I and ERA5 for the period from 09/2007 to 04/2010. Standard deviations
 716 are in brackets. Colors are used as in Table 3.

BOA	Total		DJF		MAM		JJA		SON	
# of points	149		29		48		19		53	
	Mean (σ)	Minus BSRN								
BSRN Filtered	205.4		170.3		188.1		272.7		216.0	

	(50.0)		(37.4)		(40.4)		(39.2)		(40.3)	
EUR-LR	206.2 (50.8)	0.9	171.4 (36.9)	1.0	189.8 (42.0)	1.7	273.4 (37.2)	0.7	216.2 (43.0)	0.1
CERES < 25km	194.8 (52.7)	-10.5	151.0 (32.7)	-19.3	188.7 (44.5)	0.7	281.9 (35.0)	9.1	193.1 (35.3)	-23.0
CERES nearest	195.7 (53.3)	-9.7	151.1 (34.9)	-19.3	190.4 (43.8)	2.4	280.4 (39.1)	7.6	194.5 (37.7)	-21.5
C-C-FLX R04 < 25km	201.4 (51.4)	-4.0	160.2 (38.4)	-10.1	189.4 (41.5)	1.3	272.6 (35.2)	-0.1	209.1 (41.7)	-6.9
C-C-FLX R04 nearest	200.3 (52.3)	-5.1	159.0 (40.2)	-11.4	186.9 (42.8)	-1.1	269.8 (37.6)	-2.9	210.0 (42.2)	-6.0
ERA-I	222.6 (47.2)	17.3	191.9 (44.9)	21.5	215.4 (42.7)	27.3	279.1 (38.2)	6.4	225.8 (36.8)	9.8
ERA5	200.4 (47.3)	-4.9	159.8 (33.5)	-10.5	190.6 (33.0)	2.6	279.4 (27.8)	6.6	203.3 (34.9)	-12.8
# of points	130		24		48		19		39	
	Mean (σ)	Minus BSRN								
C-C-FLX R05 < 25km	209.6 (50.7)	1.3	169.3 (36.0)	0.5	193.7 (42.4)	5.7	270.8 (38.8)	-2.0	224.0 (39.7)	-2.0
C-C-FLX R05 nearest	207.7 (52.8)	-0.6	164.8 (37.4)	-4.0	192.1 (43.0)	4.0	269.2 (37.6)	-3.6	223.3 (45.2)	-2.7

717

718

719 In Table 6, we can see that there is a wider span of annual LW BOA averages amongst

720 datasets, from 194.8 W/m² (CERES) to 222.6 W/m² (ERA-I). We restate that the lack of

721 availability of ground-based measurements during the 2006 and 2008 summers, and icing

722 screening from BSRN can induce sampling seasonal effects. Therefore, those values are not

723 expected to be used for climatological analysis. We see that the spatial sampling effect of

724 CERES and C-C-FLX fluxes (labelled as 25 km and nearest) is relatively small compared to the

725 difference with BSRN and can be explained by a mixture of cloud edges or transition with clear

726 sky. Differences remain high and comparable for all fluxes excepting CERES. The dispersion on

727 average annual values are of the order of 5 W/m², excepting CERES and ERA-I data, but those

728 on seasonal values can be about twice larger in winter, when the number of cases is reduced to

729 29. One can see that differences are larger than for summer (about 6 W/m²) when the number of

730 points is even more reduced (19). In all cases standard deviations remain high, and residual

731 uncertainties on average values (standard deviation divided by the square root of the number of

732 points) are 4 W/m² (annual average) to 8 W/m² (summer). These values have to be kept in mind

733 in the discussion of observed differences.

734 BSRN and EUR-LR agree well (within 1.7 W/m² over all seasons and better than 1W/m²

735 on average), confirming the high level of confidence of the combination of active measurements

736 with the Streamer simulations. BSRN field-of-view angular integration and EUR-LR time

737 integration are also contributing to this agreement.

738

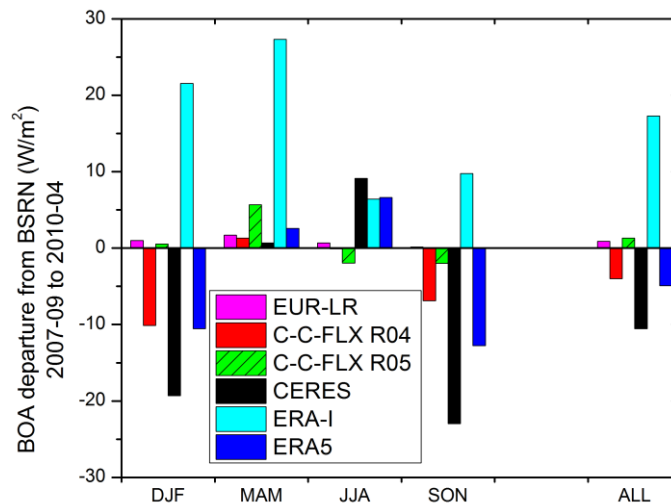
739 While CERES and C-C-FLX R04 were in good agreement in Table 3, the coincident

740 comparison showed that differences can be up to 16 W/m² in autumn and about 6.5 W/m² in741 annual mean (CERES being biased low with respect to C-C-FLX R04 by about 5W/m²). C-C-

742 FLX R05 shows reduced bias in all seasons except in spring and summer. The better

743 representation of ice and mixed-phase clouds in R05 could explain this improvement and this

744 hypothesis will be discussed in the next section. Satellite observations are lower than BSRN in
 745 all seasons and more particularly in DJF (-10 to -20 W/m²), except for C-C-FLX R05, while
 746 ERA-I is systematically much higher than BSRN for all seasons (between 6.4 to 27 W/m²) and
 747 more than 15 W/m² on average, which is consistent with the overestimation of cloud fraction at
 748 low altitude (Zib et al., 2012). The several modifications implemented for ERA5 have a
 749 significant impact as it decreases BOA LW fluxes by 22 W/m² with respect to ERA-I, and even
 750 more in winter. We found that ERA5 is in general in much better agreement with other datasets.
 751

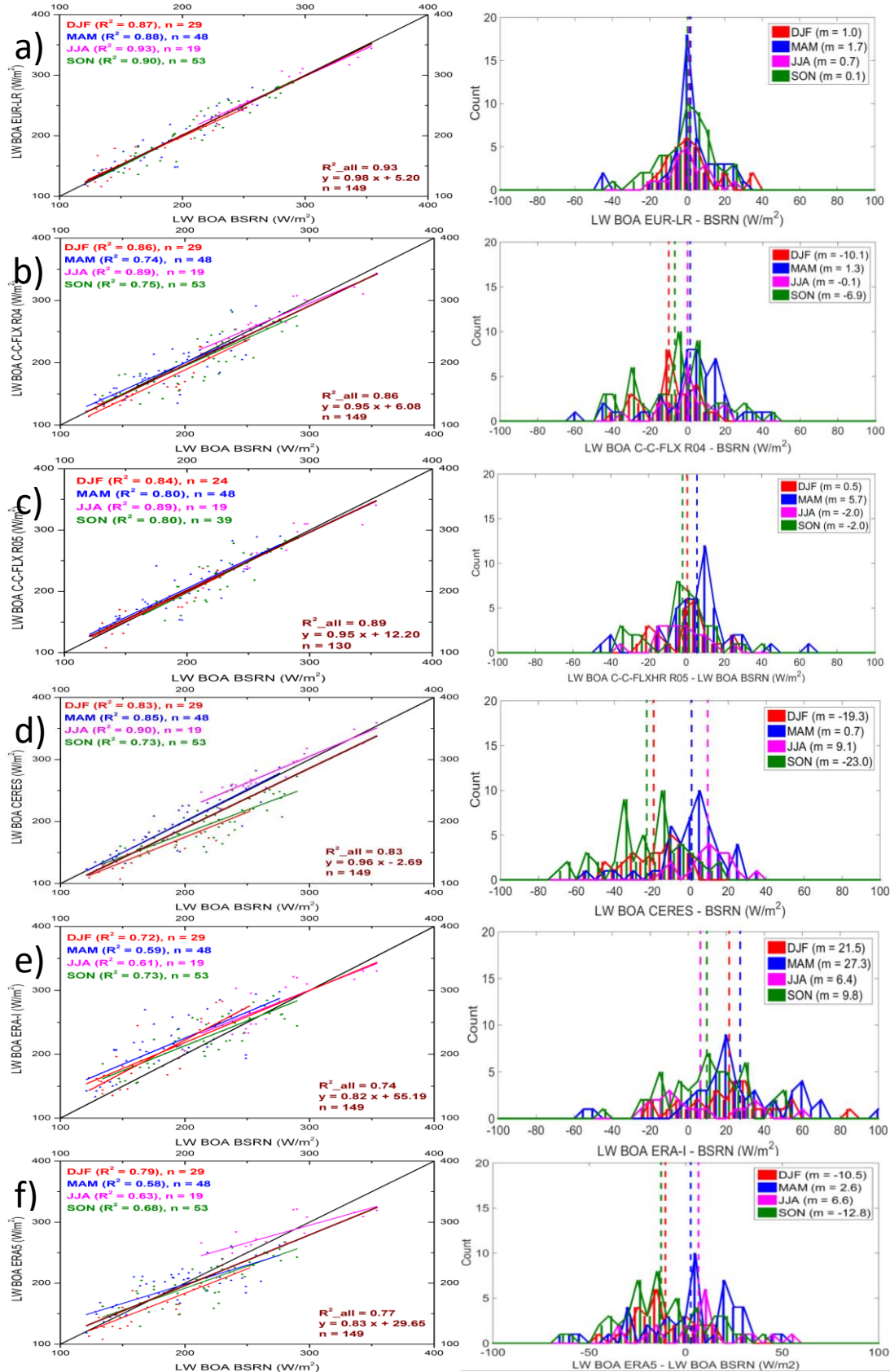


752
 753 **Figure 8.** LW BOA departure from BSRN for coincident measurements as reported in Table 6.
 754 C-C-FLX R05 bars are dashed because the comparison with BSRN is based on only 130 points.
 755

756 Figure 8 is reporting the differences observed in Table 6. It evidences that the largest
 757 differences are observed for CERES and ERA-I, with annual biases of -11 and +17 W/m²,
 758 respectively. Largest differences in autumn and winter (and spring for ERA-I), when the cloud
 759 vertical distribution was divergent. The difference observed between spring and summer and the
 760 two other seasons between C-C-FLX and CERES is statistically meaningful. A closer look at
 761 those differences will help to understand the biases.

762 4.2.2 Seasonal flux differences

763 Looking at coincident fluxes in a way similar to TOA analysis helps to identify
 764 systematic seasonal, methodological or instrumental biases compared to BSRN reference. We
 765 must be aware however that due to the footprint of satellite observations, it may be possible that
 766 although the separation distance is kept small, ground-based active instruments may not be
 767 looking at the same cloud. The reduced number of cases makes the multi-parameter analysis
 768 more difficult in terms of quantification. Fig. 9 is reporting (as in Fig. 6 for TOA fluxes) one-to-
 769 one flux comparisons and histograms of flux differences however evidences significant
 770 differences. Table 7 summarizes main parameters reported in histograms.
 771



773 **Figure 9.** Seasonal BOA downwelling LW fluxes for BRSN and EUR-LR (a) C-C-FLX R04 (b),
 774 C-C-FLX R05 (c), CERES (d), ERAI (e) and ERA5 (f) for the 149 measurements (except for
 775 R05) at the same time, between September 2007 and April 2010.

776

777 **Table 7.** Gaussian fit statistics of BOA differences between EUR-LR, C-C-FLX R04 and R05,
 778 CERES, ERA-I, ERA5 and BSRN. Note that a smaller number of points were available for R05
 779 (see Table 6).

	EUR-LR - BSRN	C-C-FLX R04 - BSRN	C-C-FLX R05 - BSRN	CERES - BSRN	ERA-I - BSRN	ERA5 - BSRN
Mean	0.8	-0.5	2.8	-6.8	2.6	-4.7
Half width at 60%	10.0	16.3	12.5	21.3	20.9	25.2
FWHM	23.5	38.0	29.2	49.6	48.6	58.7
σ (% of full width at 1/e ²)	9.9	16.1	12.4	21.1	10.6	24.9
Number of outliers (> 3 σ)	5	1	6	3	5	0

780

781 It is apparent from the histograms of BOA flux differences given in Fig. 9 that all
 782 comparisons show very large dispersions except between EUR-LR and BSRN. No significant
 783 bias and very few outliers (close to +/- 40 W/m², as evidenced from the narrower distribution)
 784 are observed in this last case. The correlation between EUR-LR and BSRN is indeed high
 785 ($R^2=0.93$, and $s = 9.9$ W/m²), but comparison of individual coincident times can be off by up to
 786 50 W/m². Those outliers are likely explained by the fact that the effective spatial resolution of
 787 active instruments after time averaging remains small compared to BSRN
 788 pyranometer/pyrgeometer, located 2.3 km away from the station, which measures hemispheric
 789 (160 degrees) LW fluxes.

790

791 The overall distributions are widely spread in almost all other cases from -60 to +60
 792 W/m². Results between C-C-FLX (R04 and R05) and BSRN show a dispersion of seasonal
 793 differences rather contained, limiting the overall bias, slightly better for R05. Figure 9c shows a
 794 smaller dispersion of C-C-FLX R05 bias vs BSRN, as compared to CERES. This confirms the
 795 advantage of lidar-radar synergy from space. But there are still high seasonal variations,
 796 especially in spring, when C-C are missing clouds below 5 km (Fig. 4). Differences between R04
 797 and R05 are minor but an overall better agreement is found for R05 and especially in winter (the
 798 R04 bias of -10 W/m² is reduced to + 0.5 W/m² for R05). Some improvements in R05 algorithm
 799 regarding ice and mixed-phase clouds could explain those differences.

800

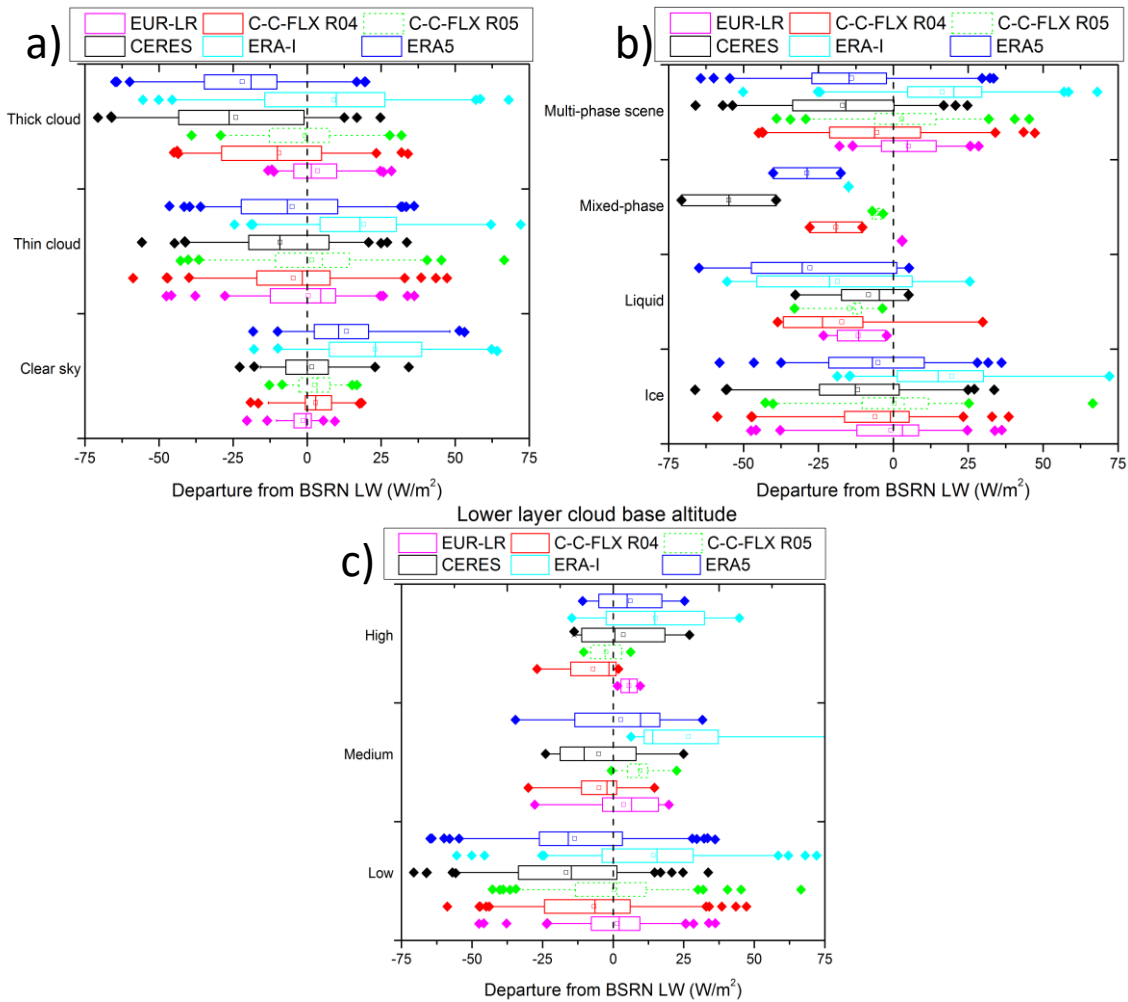
801 CERES and ERA5 show the wider spreads with a dispersion (2 sigmas) of about 50
 802 W/m². The mean biases vary from about -20 W/m² in winter and autumn to about + 10 W/m² in
 803 summer for CERES. In those winter and autumn seasons, MODIS is missing almost half of low
 804 and mid clouds (see Fig. 4). ERA5 is also biased low in winter and autumn compared to BSRN
 805 and larger in summer. This result is in agreement to what was reported in Zib et al. (2012) for
 806 Ny-Ålesund and Barrow, but using ERA-Interim. Note that those stations are, however, coastal
 807 and their cloud fraction variation is different from the one at Eureka (Shupe et al, 2011a; Shupe
 808 2011b). ERA5 corrects the BOA LW positive bias for ERA-I in winter explained by the
 809 overestimation of very low cloud in reanalyses (as reported in several papers, see Zygmuntowska

810 et al., 2012; Zib et al., 2012; Huang et al., 2017a) as seen in Fig.4. C-C-FLX and ERA5 average
 811 values show biases in winter remain high (larger than -10W/m^2) with broad distributions.

812 4.2.3 BOA differences decomposed by type of scenes

813 In this subsection, we discuss the overall relative difference of BOA fluxes to BSRN
 814 measurements as a function of the scene type as supported by ground-based lidar/radar
 815 observations.

816



817
 818 **Figure 10.** Difference of BOA LW fluxes depending on the total visible optical depth (a), phase
 819 of cloud layers (b) and bottom height of the lower layer (c). Boxes correspond to 25%, median
 820 and 75% values, thin bars show 5 and 95% and squares are used to show the mean. Outliers are
 821 also reported as coloured diamonds.

822
 823 Clear sky events (Fig 10a) are well captured by CERES, C-C-FLX and EUR-LR while
 824 the mean bias is about $+13\text{ W/m}^2$ for ERA5. For opaque clouds ($\text{COD} > 2$), CERES and C-C-
 825 FLX are biased low because they miss correct cloud base heights as identified in Fig. 4. Such
 826 clouds are expected to be mid- and low-level clouds. Indeed, high clouds that were missed by
 827 EUR-LR above opaque clouds (in the discussion about TOA) don't have a significant impact
 828 when looking at downwelling fluxes. However, it is confirmed that all other (CERES, ERA5 and

829 to a smaller extend CC-FLX R05) LW BOA fluxes are biased low for low clouds by more than
 830 20 W/m^2 with respect to BSRN BOA measurements, which appears to be the main driver of
 831 biases. The direct comparison of C-C-FLX releases (see Appendix C) confirms that R05
 832 significantly reduces the strong biases identified for low and thick clouds. Fig. 10b shows that
 833 there is a negative bias for ice layers for all dataset considered here except EUR-LR, as
 834 evidenced in Table 6. Mixed-phase (supercooled) clouds appear to be challenging for CERES as
 835 previously emphasized (Matus and L'Ecuyer, 2017). This also appears to be the case for ERA5
 836 and ERA-I, but there are rather few mixed-phase cases here to draw any definitive conclusion
 837 (Fig. 10c). As mentioned for TOA, ECMWF reanalyses are still struggling to get the water
 838 content of liquid clouds correct. This remains true for ERA5 as was the case for ERA-I
 839 (Zygmuntowska et al., 2012).

840 4.3 Summary

841 Further to B14, we have applied in this paper the approach that was laid out for cloud
 842 occurrence to the analysis of LW radiation budget at top and bottom of the atmosphere at Eureka
 843 station. The statistical analyses are enforced by an approach of separating statistical independent
 844 analysis and coincident confrontation of observations constrained by scene types. This approach
 845 controls for some sampling and observational biases that affect the analysis, and the horizontal
 846 heterogeneity was found to be a small factor. The results indicate that there is rather good
 847 agreement in TOA fluxes (within a few W/m^2), but considerably less agreement in the arguably
 848 more important BOA fluxes. Main findings are summarized in Table 8.

849
850

851 **Table 8.** Findings for each dataset

	Cloud vertical distribution	TOA	BOA
BSRN	N/A	N/A	Used as a reference
EUR-LR	Detects large number of hydrometeors close to the ground in winter. Is not able to detect high features above opaque clouds (in MAM and JJA).	Relatively good agreement (about 1 W/m^2). Issue when high clouds are not detected	Very good agreement with BSRN (bias less than 1 W/m^2)
C-C-FLX R04	Misses a significant amount of low ice clouds in winter. Good agreement with ground-based above 2km.	Always smaller than CERES (about -4 W/m^2). Could be due to footprint compared to CERES ($20 \text{ km} \times 20 \text{ km}$), that smooths TOA fluxes	Overall bias close to -5 W/m^2 . Better than CERES. Bigger bias in winter (-10 W/m^2)
C-C-FLX R05	Same as C-C-FLX R04	Smaller than CERES with larger bias compared to R04, probably due to different surface emissivity	Good agreement with BSRN (bias less than 1.5 W/m^2). Clouds are better addressed than R04 but too many mixed-phase are detected (in spring). Overall bias of about -10 W/m^2 . Differences are high in winter (about -20 W/m^2) and autumn due to a wrong detection of low clouds.
CERES	Misses clouds in all seasons, but this is more dramatic in winter over snow surface.	Used as a reference	Biggest overall bias (about $+20 \text{ W/m}^2$) larger in winter, as
ERA-I	Underestimates cloud fraction by a factor of 2. This is	Bias for clear sky due to a coarse temperature	

	somewhat compensated by the detection of clouds very close to the surface.	profile that misses temperature inversion.	caused by a bad re-analysis of cloud vertical distribution. Issues with water, ice clouds and clear sky.
ERA5	Similar to ERA-I, but a lower amount of low clouds.	In good agreement with CERES, except in summer due to inaccurate liquid water content	Overall bias close to -5 W/m^2 . Larger bias in winter (-10 W/m^2). Clear sky bias is still present (13 W/m^2) but reduced compared to ERA-I. Low liquid and ice clouds are the main sources of errors

852

853

854 For the TOA, we used CERES as a reference. From the statistical independent analysis,
855 we found results comparable to what has been previously obtained, with good agreement (better
856 than 5 W/m^2) between datasets and low biases.

856

857

858

859

860

861

862

863

864

865

866

867

868

869

870

871

872

873

874

875

876

877

878

879

880

881

882

883

884

885

886

887

888

875 Statistical and coincident analysis revealed comparable agreement in TOA with biases
876 smaller than 5 W/m^2 for all observations and analyses with respect to CERES observations. No
877 obvious trend was found on the statistical dataset. Narrow distributions are observed for satellite
878 observations, but a larger dispersion is seen on analyses, with a larger number of outliers for
879 ERA5. The difference observed appears to be mainly due to high clouds. Their occurrence is
880 slightly smaller for CERES at higher altitudes. This may be due to the fact that the altitude
881 attribution is underestimated by MODIS.

883 The results for BOA fluxes show more differences. Ground-based lidar-radar inputs to
884 radiative transfer code (streamer) give at the same time unbiased fluxes with the lower dispersion
885 with respect to BSRN reference. All other (CC-FLX, CERES and ERA5) show biases ranging
886 from 1 (C-C-FLX R05) to -10 W/m^2 (CERES and ERA5) analyzed as due to poor representation
887 of low (mixed-phase) cloud properties (liquid water content). ERA5 corrects the very large
888 positive longwave bias of $+17 \text{ W/m}^2$ observed with ERA-I, but cloud distribution remains biased

889 with respect to ground-based observations. Further improvements thus remain to be done in both
890 the retrieved fluxes from observations and analyses to better address liquid water content of
891 complex Arctic low-level clouds observed in cold seasons.

892 **5 Conclusions**

893 Existing TOA flux observing and modeling strategies are in good agreement and seem
894 sufficient. BOA fluxes on the other hand are more problematic and while there is agreement
895 between the ground-based broad-band observations and ground-based radar-lidar retrievals, these
896 are only for infrequent, single observatory sites and model and satellite methodologies to
897 characterize BOA fluxes are still insufficient for monitoring or characterizing the Arctic system.

898
899 It is essential for future operations that active sensors at ground-based sites be operated in
900 polar regions to complement space observations in order to correctly identify cloud vertical
901 profiles. Without integration of the ground-based, ongoing reference datasets into observing
902 strategies it seems unlikely that space-based observations or model projections will be able to
903 independently measure or calculate the BOA fluxes that are a critical component for
904 characterizing and monitoring the extreme environmental changes occurring in the Arctic
905 environment.

906

907 **Acknowledgments**

908 Acknowledgments are due to the Canadian Network for the Detection of Atmospheric
909 Change (CANDAC), Study of Environmental Arctic Change (SEARCH) and Environment
910 Canada for their operational support as well as radiosondes and observations data at Eureka. We
911 are grateful to Kenneth Moran from NOAA and Edwin Eloranta from University of Wisconsin–
912 Madison for providing MMCR and AHSRL data, respectively. The authors thank the CALIPSO
913 team at NASA Langley Research Center (<https://www-calipso.larc.nasa.gov/>), the ICARE data
914 Center in Lille/France (<https://www.icare.univ-lille.fr/>) and the CloudSat team at Colorado State
915 University for the availability of the level-2 data (<http://www.cloudsat.cira.colostate.edu/data-products/>). This research was supported by the Centre National d'Etudes Spatiales (CNES).
916 Acknowledgments also go to ECMWF for the ERA5 and ERA-I reanalyses and to the NASA
917 CERES team for the production of the CERES data. NASA CERES–SSF–TOA and SSF–Surface
918 products are available at <http://ceres.larc.nasa.gov/>. The BSRN dataset can be accessed from
919 World Radiation Monitoring Center at <http://www.bsrn.awi.de/>.

920
921

922 **References**

923 Abe, M., Nozawa, T., Ogura, T., & Takata, K. (2016). Effect of retreating sea ice on Arctic cloud
924 cover in simulated recent global warming. *Atmospheric Chemistry and Physics*, *16*(22),
925 14343–14356. doi:10.5194/acp-16-14343-2016

926 Ancellet, G., Pelon, J., Blanchard, Y., Quennehen, B., Bazureau, A., Law, K. S., &
927 Schwarzenboeck, A. (2014). Transport of aerosol to the Arctic: analysis of CALIOP and
928 French aircraft data during the spring 2008 POLARCAT campaign. *Atmospheric
929 Chemistry and Physics*, *14*(16), 8235–8254. <https://doi.org/10.5194/acp-14-8235-2014>

- 930 Betts, A. K., Chan, D. Z., & Desjardins, R. L. (2019). Near-Surface Biases in ERA5 Over the
931 Canadian Prairies. *Frontiers in Environmental Science*, 7. doi:10.3389/fenvs.2019.00129
- 932 Blanchard, Y., Pelon, J., Eloranta, E. W., Moran, K. P., Delanoë, J., & Sèze, G. (2014). A
933 Synergistic Analysis of Cloud Cover and Vertical Distribution from A-Train and Ground-
934 Based Sensors over the High Arctic Station Eureka from 2006 to 2010. *Journal of Applied
935 Meteorology and Climatology*, 53(11), 2553-2570. doi:10.1175/jamc-d-14-0021.1
- 936 Blanchard, Y., Royer, A., O'Neill, N. T., Turner, D. D., & Eloranta, E. W. (2017). Thin ice
937 clouds in the Arctic: Cloud optical depth and particle size retrieved from ground-based
938 thermal infrared radiometry. *Atmospheric Measurement Techniques*, 10(6), 2129-2147.
939 doi:10.5194/amt-10-2129-2017
- 940 de Boer, G., Eloranta, E. W., & Shupe, M. D. (2009). Arctic Mixed-Phase Stratiform Cloud
941 Properties from Multiple Years of Surface-Based Measurements at Two High-Latitude
942 Locations. *Journal of the Atmospheric Sciences*, 66(9), 2874-2887.
943 doi:10.1175/2009jas3029.1
- 944 Boisvert, L. N., & Stroeve, J. C. (2015). The Arctic is becoming warmer and wetter as revealed
945 by the Atmospheric Infrared Sounder. *Geophysical Research Letters*, 42(11), 4439-4446.
946 doi:10.1002/2015gl063775
- 947 Ceccaldi, M., Delanoë, J., Hogan, R. J., Pounder, N. L., Protat, A., & Pelon, J. (2013). From
948 CloudSat-CALIPSO to EarthCare: Evolution of the DARDAR cloud classification and its
949 comparison to airborne radar-lidar observations. *Journal of Geophysical Research:
950 Atmospheres*, 118(14), 7962-7981. doi:10.1002/jgrd.50579
- 951 Chan, M. A., & Comiso, J. C. (2011). Cloud features detected by MODIS but not by CloudSat
952 and CALIOP. *Geophysical Research Letters*, 38(24). doi:10.1029/2011gl050063
- 953 Chernokulsky, A., & Mokhov, I. I. (2012). Climatology of Total Cloudiness in the Arctic: An
954 Intercomparison of Observations and Reanalyses. *Advances in Meteorology*, 2012, 1–15.
955 <https://doi.org/10.1155/2012/542093>
- 956 Comiso, J. C., & Hall, D. K. (2014). Climate trends in the Arctic as observed from space. *Wiley
957 Interdisciplinary Reviews: Climate Change*, 5(3), 389–409.
958 <https://doi.org/10.1002/wcc.277>
- 959 Cox, C. J., Walden, V. P., & Rowe, P. M. (2012). A comparison of the atmospheric conditions at
960 Eureka, Canada, and Barrow, Alaska (2006-2008). *Journal of Geophysical Research:
961 Atmospheres*, 117(D12), n/a. <https://doi.org/10.1029/2011jd017164>
- 962 Cox, C. J., Walden, V. P., Rowe, P. M., & Shupe, M. D. (2015). Humidity trends imply
963 increased sensitivity to clouds in a warming Arctic. *Nature Communications*, 6(1).
964 doi:10.1038/ncomms10117

- 965 Cox, C. J., Uttal, T., Long, C. N., Shupe, M. D., Stone, R. S., & Starkweather, S. (2016). The
966 Role of Springtime Arctic Clouds in Determining Autumn Sea Ice Extent. *Journal of*
967 *Climate*, 29(18), 6581-6596. doi:10.1175/jcli-d-16-0136.1
- 968 Dee, D. P., Uppala, S. M., Simmons, A. J., Berrisford, P., Poli, P., Kobayashi, S., . . . Vitart, F.
969 (2011). The ERA-Interim reanalysis: Configuration and performance of the data
970 assimilation system. *Quarterly Journal of the Royal Meteorological Society*, 137(656),
971 553-597. doi:10.1002/qj.828
- 972 Delanoë, J., & Hogan, R. J. (2010). Combined CloudSat-CALIPSO-MODIS retrievals of the
973 properties of ice clouds. *Journal of Geophysical Research*, 115. doi:10.1029/2009jd012346
- 974 Doyle, J. G., Lesins, G., Thackray, C. P., Perro, C., Nott, G. J., Duck, T. J., . . . Drummond, J. R.
975 (2011). Water vapor intrusions into the High Arctic during winter. *Geophysical Research*
976 *Letters*, 38(12). doi:10.1029/2011gl047493
- 977 Driemel, A., Augustine, J., Behrens, K., Colle, S., Cox, C., Cuevas-Agulló, E., . . . and König-
978 Langlo, G.: (2018). Baseline Surface Radiation Network (BSRN): structure and data
979 description (1992–2017), *Earth Syst. Sci. Data*, 10, 1491–1501,
980 <https://doi.org/10.5194/essd-10-1491-2018>
- 981 Eastman, R., & Warren, S. G. (2010). Interannual Variations of Arctic Cloud Types in Relation
982 to Sea Ice. *Journal of Climate*, 23(15), 4216-4232. doi:10.1175/2010jcli3492.1
- 983 Eloranta, E. W., Uttal, T., & Shupe, M. (2007). Cloud particle size measurements in Arctic
984 clouds using lidar and radar data. *2007 IEEE International Geoscience and Remote*
985 *Sensing Symposium*. doi:10.1109/igarss.2007.4423292
- 986 English, J. M., Gettelman, A., & Henderson, G. R. (2015). Arctic Radiative Fluxes: Present-Day
987 Biases and Future Projections in CMIP5 Models. *Journal of Climate*, 28(15), 6019-6038.
988 doi:10.1175/jcli-d-14-00801.1
- 989 Fogal, P. F., Leblanc, L. M., & Drummond, J. R. (2013). The Polar Environment Atmospheric
990 Research Laboratory (PEARL): Sounding the Atmosphere at 80° North. *Arctic*, 66(3).
991 doi:10.14430/arctic4321
- 992 Grachev, A. A., Persson, P. O., Uttal, T., Akish, E. A., Cox, C. J., Morris, S. M., . . . Repina, I.
993 A. (2017). Seasonal and latitudinal variations of surface fluxes at two Arctic terrestrial
994 sites. *Climate Dynamics*, 51(5-6), 1793-1818. doi:10.1007/s00382-017-3983-4
- 995 Graham, R. M., Cohen, L., Petty, A. A., Boisvert, L. N., Rinke, A., Hudson, S. R., . . . Granskog,
996 M. A. (2017). Increasing frequency and duration of Arctic winter warming events.
997 *Geophysical Research Letters*, 44(13), 6974-6983. doi:10.1002/2017gl073395

- 998 Graham, R. M., Cohen, L., Ritzhaupt, N., Segger, B., Graversen, R. G., Rinke, A., . . . Hudson,
999 S. R. (2019a). Evaluation of Six Atmospheric Reanalyses over Arctic Sea Ice from Winter
1000 to Early Summer. *Journal of Climate*, 32(14), 4121-4143. doi:10.1175/jcli-d-18-0643.1
- 1001 Graham, R. M., Hudson, S. R., & Maturilli, M. (2019b). Improved Performance of ERA5 in
1002 Arctic Gateway Relative to Four Global Atmospheric Reanalyses. *Geophysical Research*
1003 *Letters*, 46(11), 6138-6147. doi:10.1029/2019gl082781
- 1004 Grenier, P., Blanchet, J.-P., & Muñoz-Alpizar, R. (2009). Study of polar thin ice clouds and
1005 aerosols seen by CloudSat and CALIPSO during midwinter 2007. *Journal of Geophysical*
1006 *Research*, 114(D9). doi:10.1029/2008jd010927
- 1007 Gupta, S. K., Darnell, W. L., & Wilber, A. C. (1992). A Parameterization for Longwave Surface
1008 Radiation from Satellite Data: Recent Improvements. *Journal of Applied Meteorology*,
1009 31(12), 1361-1367. doi:10.1175/1520-0450(1992)0312.0.co;2
- 1010 Gupta, S. K., Kratz, D. P., Stackhouse, P. W., Wilber, A. C., Zhang, T., & Sothcott, V. E. (2010).
1011 Improvement of Surface Longwave Flux Algorithms Used in CERES Processing. *Journal*
1012 *of Applied Meteorology and Climatology*, 49(7), 1579-1589. doi:10.1175/2010jamc2463.1
- 1013 Henderson, D. S., L'Ecuyer, T., Stephens, G., Partain, P., & Sekiguchi, M. (2013). A
1014 Multisensor Perspective on the Radiative Impacts of Clouds and Aerosols. *Journal of*
1015 *Applied Meteorology and Climatology*, 52(4), 853-871. doi:10.1175/jamc-d-12-025.1
- 1016 Henderson, D. S., & L'Ecuyer, T. (2020). CloudSat Level 2B Fluxes and Heating Rates with
1017 Lidar [2B-FLXHR-LIDAR] Process Description and Interface Control Document
1018 [Available online at
1019 [http://www.cloudsat.cira.colostate.edu/sites/default/files/products/files/2B-FLXHR-
LIDAR_PDICD.P1_R05.rev0_.pdf](http://www.cloudsat.cira.colostate.edu/sites/default/files/products/files/2B-FLXHR-
1020 LIDAR_PDICD.P1_R05.rev0_.pdf)]
- 1021 Hersbach, H., & Dee, D. (2016). ERA5 reanalysis is in production, *ECMWF Newsletter*, 147,
1022 ECMWF, Reading, UK
- 1023 Hu, Y., Winker, D., Vaughan, M., Lin, B., Omar, A., Trepte, C., Flittner, D., Yang, P., Nasiri, S.
1024 L., Baum, B., Holz, R., Sun, W., Liu, Z., Wang, Z., Young, S., Stamnes, K., Huang, J., &
1025 Kuehn, R. (2009). CALIPSO/CALIOP Cloud Phase Discrimination Algorithm. *Journal of*
1026 *Atmospheric and Oceanic Technology*, 26(11), 2293–2309.
1027 <https://doi.org/10.1175/2009jtecha1280.1>
- 1028 Huang, Y., Dong, X., Xi, B., Dolinar, E. K., & Stanfield, R. E. (2017a). The footprints of 16 year
1029 trends of Arctic springtime cloud and radiation properties on September sea ice retreat.
1030 *Journal of Geophysical Research: Atmospheres*, 122(4), 2179-2193.
1031 doi:10.1002/2016jd026020

- 1032 Huang, Y., Dong, X., Xi, B., Dolinar, E. K., Stanfield, R. E., & Qiu, S. (2017b). Quantifying the
1033 Uncertainties of Reanalyzed Arctic Cloud and Radiation Properties Using Satellite Surface
1034 Observations. *Journal of Climate*, 30(19), 8007-8029. doi:10.1175/jcli-d-16-0722.1
- 1035 Illingworth, A. J., Barker, H. W., Beljaars, A., Ceccaldi, M., Chepfer, H., Clerbaux, N., . . .
1036 Zadelhoff, G. V. (2015). The EarthCARE Satellite: The Next Step Forward in Global
1037 Measurements of Clouds, Aerosols, Precipitation, and Radiation. *Bulletin of the American*
1038 *Meteorological Society*, 96(8), 1311-1332. doi:10.1175/bams-d-12-00227.1
- 1039 IPCC (2013). *Climate Change 2013: The Physical Science Basis. Contribution of Working*
1040 *Group I to the Fifth Assessment Report of the Intergovernmental Panel on Climate Change*
1041 [Stocker, T.F., D. Qin, G.-K. Plattner, M. Tignor, S.K. Allen, J. Boschung, A. Nauels, Y.
1042 Xia, V. Bex and P.M. Midgley (eds.)]. Cambridge University Press, Cambridge, United
1043 Kingdom and New York, NY, USA, 1535 pp.
- 1044 Jun, S., Ho, C., Jeong, J., Choi, Y., & Kim, B. (2016). Recent changes in winter Arctic clouds
1045 and their relationships with sea ice and atmospheric conditions. *Tellus A: Dynamic*
1046 *Meteorology and Oceanography*, 68(1), 29130. doi:10.3402/tellusa.v68.29130
- 1047 Kay, J. E., & L'ecuyer, T. (2013). Observational constraints on Arctic Ocean clouds and radiative
1048 fluxes during the early 21st century. *Journal of Geophysical Research: Atmospheres*,
1049 118(13), 7219-7236. doi:10.1002/jgrd.50489
- 1050 Kay, J. E., L'Ecuyer, T., Chepfer, H., Loeb, N., Morrison, A., & Cesana, G. (2016). Recent
1051 Advances in Arctic Cloud and Climate Research. *Current Climate Change Reports*, 2(4),
1052 159-169. doi:10.1007/s40641-016-0051-9
- 1053 Key, J. R., & Schweiger, A. J. (1998). Tools for atmospheric radiative transfer: Streamer and
1054 FluxNet. *Computers & Geosciences*, 24(5), 443-451. doi:10.1016/s0098-3004(97)00130-1
- 1055 Kovacs, T., & McCormick, P. (2005). Cloud-Aerosol Lidar and Infrared Pathfinder Satellite
1056 Observations (CALIPSO) quidpro quo validation plan. [Available online at
1057 http://calipsovalidation.hamptonu.edu/QPQ_plan062206.htm.]
- 1058 Kratz, D. P., Gupta, S. K., Wilber, A. C., & Sothcott, V. E. (2020). Validation of the CERES
1059 Edition-4A Surface-Only Flux Algorithms. *Journal of Applied Meteorology and*
1060 *Climatology*, 59(2), 281-295. doi:10.1175/jamc-d-19-0068.1
- 1061 Lang, A., Yang, S., & Kaas, E. (2017). Sea ice thickness and recent Arctic warming.
1062 *Geophysical Research Letters*, 44(1), 409-418. doi:10.1002/2016gl071274
- 1063 L'Ecuyer, T. S., Wood, N. B., Haladay, T., Stephens, G. L., & Stackhouse, P. W. (2008). Impact
1064 of clouds on atmospheric heating based on the R04 CloudSat fluxes and heating rates data
1065 set. *Journal of Geophysical Research*, 113. doi:10.1029/2008jd009951

- 1066 Lenaerts, J. T., Van Tricht, K., Lhermitte, S., & L'ecuyer, T. S. (2017). Polar clouds and
1067 radiation in satellite observations, reanalyses, and climate models. *Geophysical Research*
1068 *Letters*, *44*(7), 3355-3364. doi:10.1002/2016gl072242
- 1069 Lesins, G., Duck, T. J., & Drummond, J. R. (2010). Climate trends at Eureka in the Canadian
1070 high arctic. *Atmosphere-Ocean*, *48*(2), 59-80. doi:10.3137/ao1103.2010
- 1071 Li, Z., & Xu, K. (2020). Arctic Clouds Simulated by a Multiscale Modeling Framework and
1072 Comparisons With Observations and Conventional GCMs. *Journal of Geophysical*
1073 *Research: Atmospheres*, *125*(1). doi:10.1029/2019jd030522
- 1074 Liu, Y., Key, J. R., Frey, R. A., Ackerman, S. A., & Menzel, W. (2004). Nighttime polar cloud
1075 detection with MODIS. *Remote Sensing of Environment*, *92*(2), 181-194.
1076 doi:10.1016/j.rse.2004.06.004
- 1077 Liu, Y., Ackerman, S. A., Maddux, B. C., Key, J. R., & Frey, R. A. (2010). Errors in Cloud
1078 Detection over the Arctic Using a Satellite Imager and Implications for Observing
1079 Feedback Mechanisms. *Journal of Climate*, *23*(7), 1894-1907. doi:10.1175/2009jcli3386.1
- 1080 Liu, Y., Key, J. R., Liu, Z., Wang, X., & Vavrus, S. J. (2012). A cloudier Arctic expected with
1081 diminishing sea ice. *Geophysical Research Letters*, *39*(5). doi:10.1029/2012gl051251
- 1082 Liu, Y., & Key, J. R. (2016). Assessment of Arctic Cloud Cover Anomalies in Atmospheric
1083 Reanalysis Products Using Satellite Data. *Journal of Climate*, *29*(17), 6065-6083.
1084 doi:10.1175/jcli-d-15-0861.1
- 1085 Liu, Y., Shupe, M. D., Wang, Z., & Mace, G. (2017). Cloud vertical distribution from combined
1086 surface and space radar–lidar observations at two Arctic atmospheric observatories.
1087 *Atmospheric Chemistry and Physics*, *17*(9), 5973-5989. doi:10.5194/acp-17-5973-2017
- 1088 Liu, Y., Key, J. R., Vavrus, S., & Woods, C. (2018). Time Evolution of the Cloud Response to
1089 Moisture Intrusions into the Arctic during Winter. *Journal of Climate*, *31*(22), 9389-9405.
1090 doi:10.1175/jcli-d-17-0896.1
- 1091 Loeb, N. G., Wielicki, B. A., Doelling, D. R., Smith, G. L., Keyes, D. F., Kato, S., . . . Wong, T.
1092 (2009). Toward Optimal Closure of the Earth's Top-of-Atmosphere Radiation Budget.
1093 *Journal of Climate*, *22*(3), 748-766. doi:10.1175/2008jcli2637.1
- 1094 Loeb, N. G., Doelling, D. R., Wang, H., Su, W., Nguyen, C., Corbett, J. G., . . . Kato, S. (2018).
1095 Clouds and the Earth's Radiant Energy System (CERES) Energy Balanced and Filled
1096 (EBAF) Top-of-Atmosphere (TOA) Edition-4.0 Data Product. *Journal of Climate*, *31*(2),
1097 895-918. doi:10.1175/jcli-d-17-0208.1
- 1098 Mariage, V., Pelon, J., Blouzon, F., Victori, S., Geyskens, N., Amarouche, N., . . . Provost, C.
1099 (2017). IAOOS microlidar-on-buoy development and first atmospheric observations

- 1100 obtained during 2014 and 2015 arctic drifts. *Optics Express*, 25(4).
1101 doi:10.1364/oe.25.000a73
- 1102 McArthur L. J. B. (2005). Baseline Surface Radiation Network (BSRN). Operations Manual
1103 Version 2.1, WCRP-121, WMO/TD-No. 1274
- 1104 McBean, G., and Coauthors (2005). *Arctic climate: Past and present. Arctic Climate Impact*
1105 *Assessment Scientific Rep.*, Cambridge University Press, 21–60. [Available online at
1106 http://www.acia.uaf.edu/PDFs/ACIA_Science_Chapters_Final/ACIA_Ch02_Final.pdf.]
- 1107 Matus, A. V., & L'ecuyer, T. S. (2017). The role of cloud phase in Earth's radiation budget.
1108 *Journal of Geophysical Research: Atmospheres*, 122(5), 2559-2578.
1109 doi:10.1002/2016jd025951
- 1110 Palerme, C., Claud, C., Wood, N. B., L'ecuyer, T., & Genthon, C. (2019). How Does Ground
1111 Clutter Affect CloudSat Snowfall Retrievals Over Ice Sheets? *IEEE Geoscience and*
1112 *Remote Sensing Letters*, 16(3), 342-346. doi:10.1109/lgrs.2018.2875007
- 1113 Palm, S. P., Strey, S. T., Spinhirne, J., & Markus, T. (2010). Influence of Arctic sea ice extent on
1114 polar cloud fraction and vertical structure and implications for regional climate. *Journal of*
1115 *Geophysical Research*, 115(D21). doi:10.1029/2010jd013900
- 1116 Provost C., Pelon, J., Sennéchaël, N., Calzas, M., Blouzon, F., et al. (2015). IAOOS (Ice -
1117 Atmosphere - Arctic Ocean Observing System, 2011-2019). *Mercator Ocean Quarterly*
1118 *Newsletter*, Mercator Ocean, Special Issue with ICE-ARC, pp.13-15
- 1119 Rahn, K. A. (1981). Relative importances of North America and Eurasia as sources of arctic
1120 aerosol. *Atmospheric Environment (1967)*, 15(8), 1447-1455. doi:10.1016/0004-
1121 6981(81)90351-6
- 1122 Sedlar, J., Tjernström, M., Mauritsen, T., Shupe, M. D., Brooks, I. M., Persson, P. O., . . .
1123 Nicolaus, M. (2010). A transitioning Arctic surface energy budget: The impacts of solar
1124 zenith angle, surface albedo and cloud radiative forcing. *Climate Dynamics*, 37(7-8), 1643-
1125 1660. doi:10.1007/s00382-010-0937-5
- 1126 Sedlar, J., Shupe, M. D., & Tjernström, M. (2012). On the Relationship between
1127 Thermodynamic Structure and Cloud Top, and Its Climate Significance in the Arctic.
1128 *Journal of Climate*, 25(7), 2374-2393. doi:10.1175/jcli-d-11-00186.1
- 1129 Serreze, M. C., & Barry, R. G. (2011). Processes and impacts of Arctic amplification: A research
1130 synthesis. *Global and Planetary Change*, 77(1-2), 85-96.
1131 doi:10.1016/j.gloplacha.2011.03.004

- 1133 Serreze, M. C., & Barry, R. G. (2014). *The Arctic climate system*. New York, NY: Cambridge
1134 University Press.
- 1135 Shupe, M. D. (2007). A ground-based multisensor cloud phase classifier. *Geophysical Research*
1136 *Letters*, 34(22). doi:10.1029/2007gl031008
- 1137 Shupe, M. D., Walden, V. P., Eloranta, E., Uttal, T., Campbell, J. R., Starkweather, S. M., &
1138 Shiobara, M. (2011a). Clouds at Arctic Atmospheric Observatories. Part I: Occurrence and
1139 Macrophysical Properties. *Journal of Applied Meteorology and Climatology*, 50(3), 626-
1140 644. doi:10.1175/2010jamc2467.1
- 1141 Shupe, M. D. (2011b). Clouds at Arctic Atmospheric Observatories. Part II: Thermodynamic
1142 Phase Characteristics. *Journal of Applied Meteorology and Climatology*, 50(3), 645-661.
1143 doi:10.1175/2010jamc2468.1
- 1144 Shupe, M. D., Persson, P. O., Brooks, I. M., Tjernström, M., Sedlar, J., Mauritsen, T., . . . Leck,
1145 C. (2013). Cloud and boundary layer interactions over the Arctic sea ice in late summer.
1146 *Atmospheric Chemistry and Physics*, 13(18), 9379-9399. doi:10.5194/acp-13-9379-2013
- 1147 Shupe, M. D., Tjernstrom, M., & Persson, P. O. G., (2015a). Challenge of Arctic clouds and their
1148 implications for surface radiation [in "State of the Climate in 2014"], *Bull. Amer. Meteor.*
1149 *Soc.*, 96(7), S130-S131
- 1150 Shupe, M. D., Turner, D. D., Zwink, A., Thieman, M. M., Mlawer, E. J., & Shippert, T. (2015b).
1151 Deriving Arctic Cloud Microphysics at Barrow, Alaska: Algorithms, Results, and
1152 Radiative Closure. *Journal of Applied Meteorology and Climatology*, 54(7), 1675-1689.
1153 doi:10.1175/jamc-d-15-0054.1
- 1154 Stephens, G., Winker, D., Pelon, J., Trepte, C., Vane, D., Yuhas, C., . . . Lebsock, M. (2018).
1155 CloudSat and CALIPSO within the A-Train: Ten Years of Actively Observing the Earth
1156 System. *Bulletin of the American Meteorological Society*, 99(3), 569-581.
1157 doi:10.1175/bams-d-16-0324.1
- 1158 Uttal, T., Curry, J. A., Mcphee, M. G., Perovich, D. K., Moritz, R. E., Maslanik, J. A., . . .
1159 Grenfeld, T. C. (2002). Surface Heat Budget of the Arctic Ocean. *Bulletin of the American*
1160 *Meteorological Society*, 83(2), 255-275. doi:10.1175/1520-0477(2002)0832.3.co;2
- 1161 Uttal, T., Starkweather, S., Drummond, J. R., Vihma, T., Makshtas, A. P., Darby, L. S., . . .
1162 Intrieri, J. M. (2016). International Arctic Systems for Observing the Atmosphere: An
1163 International Polar Year Legacy Consortium. *Bulletin of the American Meteorological*
1164 *Society*, 97(6), 1033-1056. doi:10.1175/bams-d-14-00145.1
- 1165 Wang, C., Graham, R. M., Wang, K., Gerland, S., & Granskog, M. A. (2019). Comparison of
1166 ERA5 and ERA-Interim near-surface air temperature, snowfall and precipitation over
1167 Arctic sea ice: Effects on sea ice thermodynamics and evolution. *The Cryosphere*, 13(6),
1168 1661-1679. doi:10.5194/tc-13-1661-2019

1169 Wielicki, B. A., Barkstrom, B. R., Harrison, E. F., Lee, R. B., Smith, G. L., & Cooper, J. E.
1170 (1996). Clouds and the Earth's Radiant Energy System (CERES): An Earth Observing
1171 System Experiment. *Bulletin of the American Meteorological Society*, 77(5), 853-868.
1172 doi:10.1175/1520-0477(1996)0772.0.co;2

1173 Zib, B. J., Dong, X., Xi, B., & Kennedy, A. (2012). Evaluation and Intercomparison of Cloud
1174 Fraction and Radiative Fluxes in Recent Reanalyses over the Arctic Using BSRN Surface
1175 Observations. *Journal of Climate*, 25(7), 2291-2305. doi:10.1175/jcli-d-11-00147.1

1176 Zygmuntowska, M., Mauritsen, T., Quaas, J., & Kaleschke, L. (2012). Arctic Clouds and Surface
1177 Radiation – a critical comparison of satellite retrievals and the ERA-Interim reanalysis.
1178 *Atmospheric Chemistry and Physics*, 12(14), 6667-6677. doi:10.5194/acp-12-6667-2012

1179

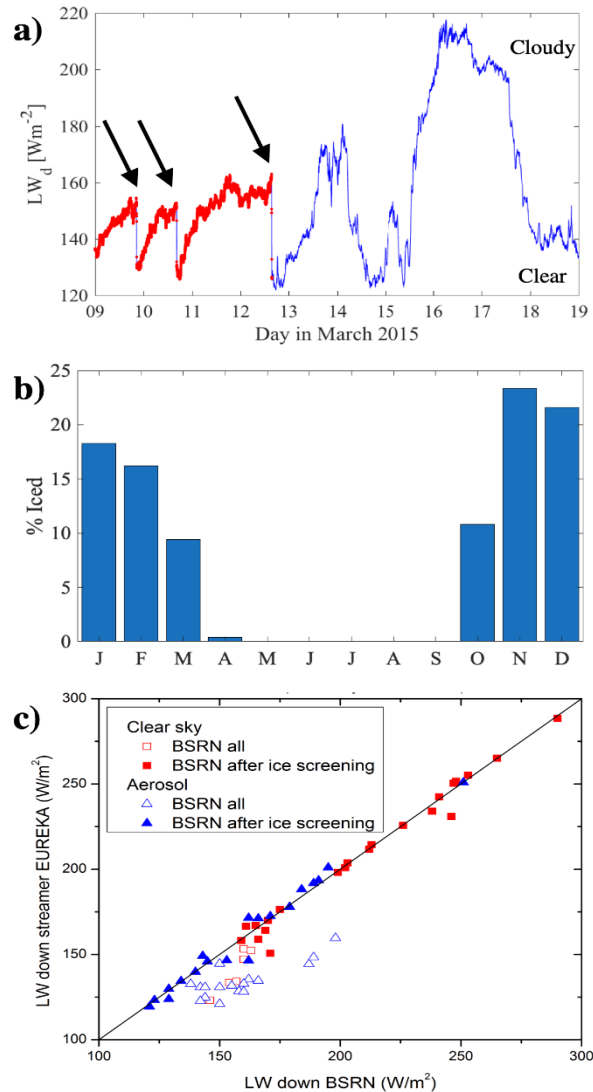
1180 **Appendix A: Screening frost events**

1181 LWD measured by the BSRN station at Eureka was frequently affected by the presence
1182 of ice on the sensor dome, likely in the form of frost or rime. Though the signal caused by ice is
1183 difficult to distinguish from the signal caused by clouds, occurrences of icing in the data set were
1184 identifiable by the characteristic "growth curve" (a rapid increase in signal that plateaus as the
1185 coverage of ice over and optical depth of the ice increases) over the course of 12-48 hours
1186 followed by abrupt decreases in flux when the domes were cleaned by the tech (e.g., Figure
1187 A1a). The data set was visually screened for these occurrences and the suspect data removed.
1188 Figure A1b shows the composite percentage of data for each month of the year when data was
1189 removed, indicating that ice occurs ~10-25% of the time from October through March, but that it
1190 rarely occurs in other months.

1191

1192 To further ensure data quality of the BSRN data used for the direct comparisons with the
1193 satellite products, additional screening was performed on coincident cases used for analysis. This
1194 screening revisited to possibility of icing and also investigated whether cloud cover was
1195 sufficiently uniform so as to be representative of the fields of view from both the surface and
1196 satellite measurements. Outliers in the comparison (examples in Figure A1c) received this
1197 further scrutiny; the signal was reviewed again for evidence of icing and the tech's logbook notes
1198 were reviewed. Additionally, observations from a nearby vertically-pointing cloud radar (refer to
1199 Shupe et al. 2011a for instrument details) were reviewed for evidence of temporally-
1200 heterogeneous cloud cover (e.g., frontal systems passing near in time to overpass) that would
1201 suggest a scene mismatch as an explanation for the discrepancy between the surface and satellite
1202 observations.

1203



1204

1205 **Figure A1.** (a) Example of the signal caused by icing of the upward-facing pyrgeometer (LWD

1206 measurement) occurring during clear sky on three consecutive days in March 2015 at Eureka.

1207 Red dots denote the identifications of ice. The arrows point to the times when the technician

1208 cleaned the ice from the dome. The magnitude of the signal caused by the icing is similar to the

1209 variability cause by alternating clear-sky and cloudy periods between day 13 and 19. (b) Percent

1210 of time in each month (aggregate 2007-2011) when ice was identified and removed. (c) Ice

1211 screening results of coincident measurements from BSRN and simulations EUR-LR. The colors

1212 indicate the scene classification based on ground-based observations, where aerosol meaning that

1213 an aerosol layer with an optical depth larger than 0.2 was observed. Suspect behavior (open

1214 symbols) were revisited. The screening method helps to remove suspicious measurements

1215 (184572 cases representing about 8% of the whole dataset). The screened observations are not

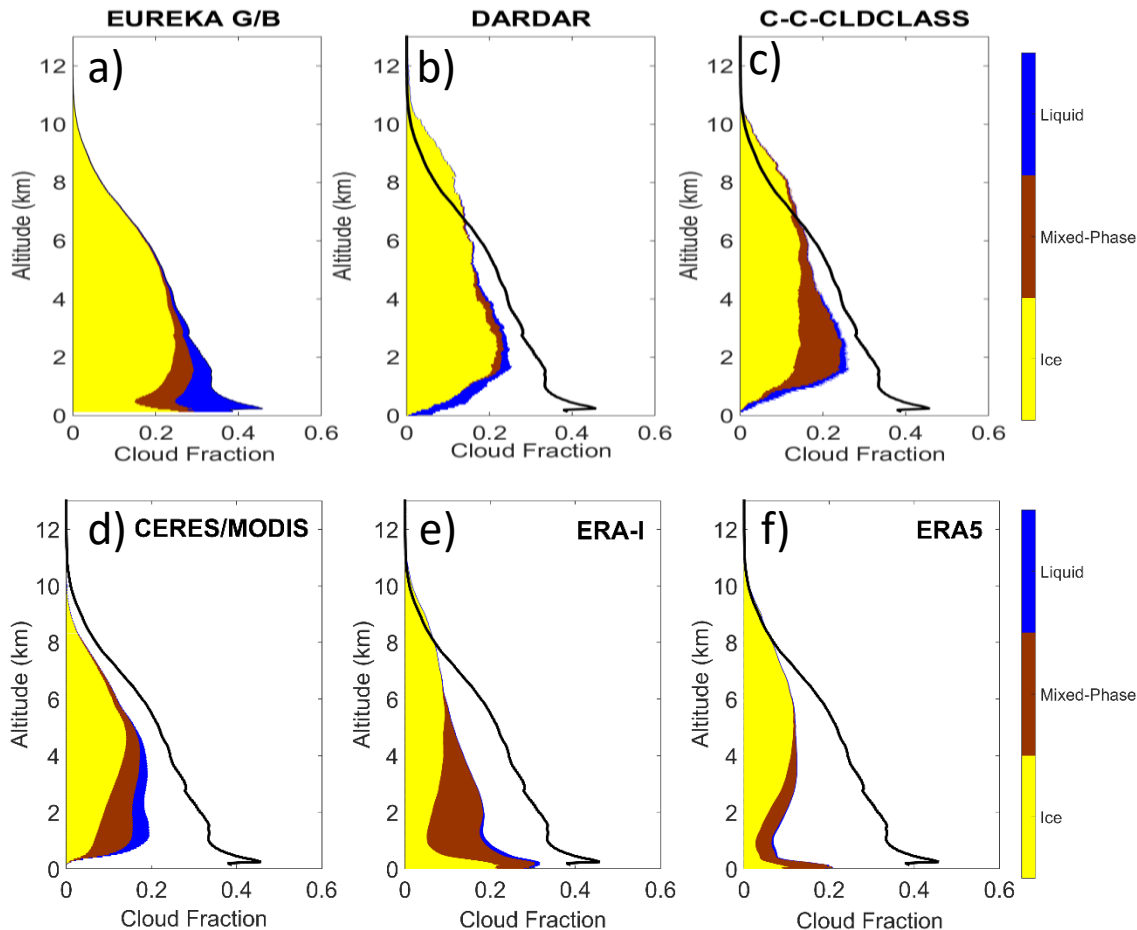
1216 used in our trend analysis, but allows to get a reliable reference dataset for comparisons LW TOA

1217 departure from CERES as reported in Table 4. C-C-FLX R05 comparison with CERES is based

1218 on only 221 points (249 for R04 and other datasets).

1219 **Appendix B: Annual cloud vertical distribution**

1220 Cloud vertical distribution and cloud type are indeed key parameters in flux calculations.
 1221 We here compare input vertical profiles from satellite and ground-based measurements and
 1222 reanalysis between June 2006 and May 2010 (green lines in Figure 2). In this paper, as a
 1223 conclusion from B14, the EUR-LR is considered to be the reference for the low-level clouds,
 1224 whereas space radar-lidar data are considered as such for upper level data (> 6 km).
 1225



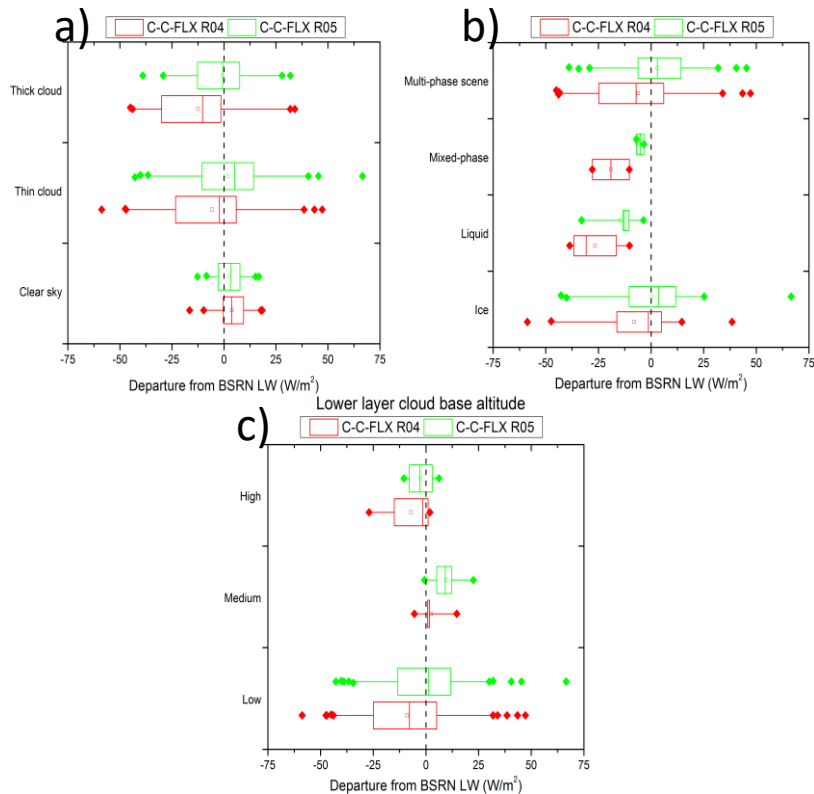
1226 **Figure B1.** Cumulated vertical cloud-type distribution between June 2006 and May 2010 for all
 1227 the independent datasets (a) EUR-LR; b) DARDAR; c) CloudSat 2B-CLDCLASS-LIDAR R05
 1228 (C-C); d) MODIS; e) ERA-I; f) ERA5 at less than 25 km from the station as compared to
 1229 ground-based observations at EUREKA (solid line) given as the total cloud occurrence in Fig.
 1230 4a. We have reported EUR-LR total cloud fraction from FigB1a in all other figures B1b, c, d, e, f
 1231
 1232

1233 DARDAR and C-C cloud vertical distributions are very close to EUR-LR above 2 km.
 1234 MODIS are close to DARDAR, although MODIS is slightly more biased below 4 km. As
 1235 detailed in B14, very low clouds are difficult to address from space, and this is confirmed here
 1236 from DARDAR, C-C and MODIS for which cloud fractions are much lower than EUR-LR
 1237 observations below 2 km. DARDAR and C-C are close although DARDAR gives a higher
 1238 amount of ice clouds and less mixed-phase clouds. The finer vertical resolution for DARDAR
 1239 (60 m) compared to C-C (240 m) might explain this difference as C-C would not be able to
 1240 distinguish different water phases within one radar gate. ERA-I misses a large fraction of cloud

1241 below 8 km (Liu and Key, 2016). ERA5 appears to have a bias larger than ERA-I, and the
 1242 fraction of mixed-phased clouds is observed to be much smaller. All behaviours are however
 1243 rather similar, with more or less important bias in the vertical cloud fraction but significant
 1244 biases below 2 km.

1245 Appendix C: Comparison of LW BOA CloudSat flux products R04 and R05

1246 A comparison is made on cloud types and cloud properties for 130 cases of observations
 1247 with C-C-FLX R04 and R05 products.
 1248



1249 **Figure C1.** Difference of BOA LW fluxes of C-C-FLX R04 (red) and C-C-FLX R05 (green)
 1250 depending on the total visible optical depth (a), phase of cloud layers (b) and bottom height of
 1251 the lower layer (c). Boxes correspond to 25%, median and 75% values, thin bars show 5 and
 1252 95% and squares are used to show the mean. Outliers are also reported as coloured diamonds.
 1253
 1254

1255 Figure C1 shows box plots of CloudSat products departure from BSRN for 130
 1256 coincident cases to evaluate the impact of the changes in R05. Those changes were made to
 1257 improve the representation of cloud properties (cloud detection, supercooled liquid and ice
 1258 clouds microphysical properties) and consistency with CALIPSO cloud products along with
 1259 updated data ingested. We found that R05 significantly reduces the strong biases identified for
 1260 low and thick clouds. It confirms the importance of resolving cloud phase vertical distribution in
 1261 surface flux calculations.